Since January 2020 Elsevier has created a COVID-19 resource centre with free information in English and Mandarin on the novel coronavirus COVID-19. The COVID-19 resource centre is hosted on Elsevier Connect, the company's public news and information website.

Journal of CO2 Utilization 59 (2022) 101970

Contents lists available at ScienceDirect

Journal of CO2 Utilization

journal homepage: www.elsevier.com/locate/jcou

Management of surgical mask waste to activated carbons for CO_2 capture

Jarosław Serafin [a,*], Joanna Sreńscek-Nazzal [b,*], Adrianna Kamińska [b], Oliwia Paszkiewicz [c], Beata Michalkiewicz [b]

[a] Institute of Energy Technologies, Department of Chemical Engineering and Barcelona Research Center in Multiscale Science and Engineering, Universitat Politècnica de Catalunya, EEBE, Eduard Maristany 16, 08019 Barcelona, Spain

[b] West Pomeranian University of Technology in Szczecin, Faculty of Chemical Technology and Engineering, Department of Catalytic and Sorbent Materials Engineering, Piastów Ave. 42, 71-065 Szczecin, Poland

[c] Department of Chemical and Process Engineering, West Pomeranian University of Technology in Szczecin, Piastow 42, 71-065 Szczecin, Poland

ARTICLE INFO

Keywords:
Activated carbons
Surgical mask waste
Polymer management
COVID-19, CO_2 adsorption

ABSTRACT

The worldwide COVID-19 pandemic has resulted in a huge amount of face masks being used up and thrown away, resulting in increased environmental pollution and infection risks. In our work, we have developed a highly efficient process of neutralizing face mask waste into a useful carbon material. Then, the prepared activated carbon was used for CO_2 adsorption studies. A series of activated carbons from face masks used as a precursor were synthesized using KOH and the activation temperature was in the range of 600–800 °C. All materials were characterized by well-developed porosity. The influence of activation temperature on the textural properties of prepared activated carbons and their adsorption abilities were investigated. The highest CO_2 adsorption was received for the M_800 carbon and it was 3.91 mmol/g at the temperature of 0 °C and the pressure of 1 bar. M_800 carbon exhibited also high selectivity of CO_2 over N_2. Seven equilibrium isotherms were applied to the experimental data to find out the best fit (Langmuir, Freundlich, Sips, Toth, Unilan, Fritz-Schlunder and Radke-Prausnitz isotherms). The presented research provides an environmentally friendly and cost-effective method of recycling waste masks into a valuable product in the form of carbon and its potential use in the absorption of harmful CO_2 influencing the greenhouse effect.

1. Introduction

Nowadays, one of the huge problems which should be resolved is global warming. Carbon dioxide is the primary greenhouse gas emitted as a result of human activities. For CO_2 adsorption, various porous materials are used, including zeolites [1], modified TiO_2 [2], metal organic frameworks MOF [3], carbon spheres [4] or just activated carbons, which are particularly important because they have a very large specific surface, well-developed microporosity, often defined pore morphology, remarkable chemical, thermal properties and good affinity resistance to various types of pollutants [5].

Zeolites are highly ordered microporous crystalline materials. A number of their properties such as pore size and architecture or chemical composition affect their adsorption performance. They were intensively investigated as quite high CO_2 adsorption was achieved [6]. In terms of practical applications, moisture is a big problem to zeolite based adsorbents·H_2O is an important component of flue gas and some other industrial gases, and it competes with CO_2. From a thermodynamic viewpoint, the adsorption of CO_2 in the presence of H_2O is not favored in zeolites [7]. In addition, in the presence of CO_2, the acidic conditions may cause dealumination of zeolite structures, leading to a partial or total destruction of the framework [8].

MOFs are network solids composed of metal ion or metal cluster vertices linked by organic spacers. Although MOFs have very high capacity at high pressures, at atmospheric pressures their capacity is lower as compared to other physical sorbents. Further research is needed to develop MOFs targeting key material properties such as stability, multicycle applicability and competitive sorption [9]. In particular, the stability of a framework toward long-term exposure to water vapor is a critical issue in determining its suitability for CO_2 capture from flue gas [10].

Activated carbons have advantages over other CO_2 adsorbents because of their wide availability, low cost and high thermal stability [6]. Owing to their low cost, high surface area, high amenability to pore structure modification and surface functionalization, and relative ease of regeneration, carbon-based materials are considered to be some of the

* Corresponding authors.
E-mail addresses: jaroslaw.serafin@upc.edu (J. Serafin), jsrenscek@zut.edu.pl (J. Sreńscek-Nazzal).

https://doi.org/10.1016/j.jcou.2022.101970
Received 5 January 2022; Received in revised form 21 February 2022; Accepted 5 March 2022
Available online 13 March 2022

most promising adsorbents for capturing CO_2 [11]. In spite of the hydrophobic character of carbon-based adsorbents, their CO_2 adsorption ability is adversely affected by the presence of water vapor [12]. To decrease the cost of adsorbents, cheaper carbon resources such as biomass and waste can be selected. The application of surgical mask waste described in this paper is the way for waste valorization and for utilization of hazardous waste.

The characteristic property of carbon materials is that they have a well-developed internal structure consisting of pores of various sizes and shapes. Depending on the diameter length, these pores are divided into micropores, mesopores and macropores, which play significantly different roles in adsorption processes [13]. Thus, the porous structure of active carbons significantly affects the sorption properties and thus determines the possibilities of their use. A significant advantage of active carbons as adsorbents is the fact that their structure can be easily modified by using various raw materials, binders, carbonization or activation parameters, thanks to which it is possible to obtain several types of activated carbons made of the same raw material.

Currently, there are many methods of capturing and separating carbon dioxide from the flue gas stream, both used, implemented and still being developed. The most commonly used methods are absorption - chemisorption of CO_2 in amine solutions. However, these methods are becoming relatively too costly and ineffective. Among the more modern methods, it is worth mentioning adsorption and membrane technologies, CO_2 separation in the oxygen combustion technology or combustion in a chemical loop (chemical loo-ping). Adsorption methods seem to be particularly promising due to relatively low operating costs, high levels of recovery and purity of the captured carbon dioxide. Among the adsorption methods, several techniques can be listed, due to the method of regeneration of the adsorbent bed, such as [14–19]: TSA - variable temperature adsorption; PSA - pressure swing adsorption, PTSA - pressure swing and temperature swing adsorption; VPSA - pressure swing adsorption with the use of vacuum for regeneration ration; ESA - adsorption with the use of low voltage electric current; RPSA - pressure swing adsorption with a fast pressure jump; URPSA - pressure swing adsorption with an ultrafast pressure jump. The PSA, PTSA and VPSA methods seem to be the most promising, due to the degree of research advancement and the estimated costs of adsorbent regeneration.

Fine particles with large surface area and unique properties are very attractive for many applications. The control of their size, shape, consistency, and composition is necessary and important to ensure their specific commercial applications and meet application requirements [20]. Therefore, recently there has been an increased interest in the production of specific adsorbent materials, characterized by fine or ultrafine particles. As Raganati and Ammendola [21] mention, these materials can quite easily serve as a substrate for the production of sorbents with an unusual affinity for CO_2 molecules [22]. Their advantages include their physicochemical properties and the ease of their modification [23]. However, an important fact is that most of the sorbents currently available on the market are produced in the form of powders [18,19,24], which requires the development of new technologies for processing large particles in large quantities. One of these techniques is fluidization. Its advantages include: a large surface area and efficiency of gas-solid contact, high heat / mass transfer coefficients, relatively easy control of the bed temperature uniformity, high flow properties of particles, flexibility in terms of types of powders to be processed, and suitable for large-scale applications [25]. However, the disadvantage of this technique is the fact that fine or ultra-fine particles, i.e. those belonging to Geldart group C cannot be fluidized under normal fluidization conditions due to their internal cohesion [26]. To solve this problem, the research group from Naples developed a sonic assisted fluidized bed (SAFB) reactor for testing the fluidization behavior of fine/ultrafine cohesive powders at atmospheric pressure and in low and high-temperature chemical processes [27,28].

Many studies have noticed that in the case of CO_2 adsorption, there is an effect of correlation between the textural properties of carbon materials and their CO_2 adsorption capacity. Typically, CO_2 adsorption has been associated with the specific surface area value [29], total pore volume [30] or micropore volume [31].

Many activated carbons with a high CO_2 adsorption capacity are obtained through the use of KOH chemical activation [32–34]. Currently, the goal is produce activated carbons from the conversion of used materials in order to minimize waste.

For example, activated carbon as a CO_2 sorbent was obtained from waste tea [35] where the adsorption of CO_2 at 30 °C and 1 bar was 2.5 mmol/g, from waste polymers resulting in carbonization of carbon on which CO_2 adsorption at 25 °C and 1 bar was up to 3.0 mmol/g [36], or from coconut shells that showed CO_2 uptake at 1 bar up to 3.7 mmol/g at 25 °C and up to 5.12 mmol/g at 0 °C. Also, coals from biomass such as bamboo, starch or sawdust were used as carbon precursors for CO_2 adsorption, showing a CO_2 capacity of approx. 1.4–4.8 mmol/g at 25 °C and 1 bar [32,37].

Recently, since December 2019, the world's attention has been drawn to the emergence of a new disease (COVID-19) caused by the SARS-CoV-2 coronavirus [38]. In order to reduce the spread of the health risk associated with COVID-19, both medical staff and the general public have been advised to use personal protective equipment, such as surgical masks, face masks, face shields, gowns and gloves [39].

During the COVID-19 epidemic, there has been a surge in the use of face masks, gloves, and hand sanitizer bottles, which are mostly made of plastic, leading to an increase in waste from these types of materials. If these products are not handled properly or disposed of, they may still contain contamination with pathogens considered hazardous waste and pose a high risk of infection to medical personnel and the public due to the spread of these pathogens into the environment. Many countries around the world are struggling with the management of plastic waste, which is a threat to the environment [40].

Today, the increasing demand for protective disposable face masks to protect against virus infection has unfortunately increased the amount of this type of plastic waste. What is more, used masks are often not properly collected and neutralized, only dropped by people on the streets, where they create piles of rubbish in public places. Therefore, one should strive to select an alternative and most environmentally friendly method of dealing with disposable face masks. Therefore, it is extremely important to find an appropriate way of how to manage this type of waste.

Our work proposes an effective and cheap process for converting waste face masks into activated carbon as an added value, which is the first instance of using the material as an adsorbent in the CO_2 capture process. Waste masks are transformed into a valuable carbon material in a high-temperature, one-step carbonization process combined with chemical activation of KOH. The influence of the textural parameters of the carbons in correlation with the amount of carbon dioxide adsorption was investigated. In addition, the influence of the activation temperature on the properties of carbons obtained was systematically investigated. Moreover, the adsorption equilibrium data for the best CO_2 sorbents were also presented and fitted to Langmuir, Freundlich, Sips, Toth, Radlich-Peterson, Unilan, Fritz-Schlunder, Radke-Prausnitz, Temkin and Pyzhev, as well as Dubinin-Radushkevich equations. The obtained data can be useful for the design of CO_2 separation process.

2. Materials and methods

2.1. Preparation of activated carbon from a disposable mask

The precursor to the production of activated carbons were disposable face masks manufactured by AP PROPERTY S.A. (Poland). According to the literature the average carbon content of the precursor material – surgical mask was 75.9% [41,42]. A saturated KOH solution was used as the chemical activating agent. After elimination of the wire and rubber strip the major part of face mask has been cut into pieces and treated with an activator at ambient temperature for 3 h. The mass ratio of KOH:

precursor was 1: 1. After drying, the material was ground. Carbonization coupled with activation was performed in a tube furnace using temperatures ranging from 600 to 800 °C under nitrogen flow. The sample was heated with a rate of 10 °C min^{-1} to reach the processing temperature. That temperature was maintained for 1 h. After cooling, the resulting product was washed with distilled water, then with 1 mol/dm^3 hydrochloric acid and again with distilled water until the pH was neutral. The resulting material was finally dried in an oven at 200 °C overnight. The obtained carbon (AC) from disposable face masks was named as: M (mask) _T (temperature). The temperature was initially changed every 100 °C. After analysis of textural properties it was found that the activation should be carried out every 50 °C.

2.2. Characterization of carbon materials

The X-ray fluorescence energy dispersion spectrometer (EDXRF) Epsilon3 type (Panalytical, Almelo, The Netherlands, 2011) was used to determine the metal content in the carbon materials.

The textural properties of activated carbons were determined by nitrogen adsorption/desorption at −196 °C. This characterization was carried out on an automated volumetric apparatus Quadrasorb Evo™ Gas Sorption analyzer (Anton Paar, St Albans, UK; previously Quantachrome Instruments, USA, 2014). All samples were out-gassed at 250 °C overnight prior to the measurements. The porous structure was determined from the N_2 sorption isotherms at the temperature of −196 °C. The specific surface areas (S_{BET}) were calculated using the Brunauer–Emmett–Teller (BET) equation using a relative pressure of 0.05–0.20. The total pore volume (V_{tot}) was calculated from the nitrogen amount adsorbed at a relative pressure, $p / p_0 = 0.99$. The micropore volume ($V_{mic,N2}$) was determined using the DFT method (density functional theory).

CO_2 adsorption at temperature 0 °C was used to measure micropores with smaller diameters (0.3–1.47 nm). The pore size distribution was determined by the DFT method using the NLDFT model for CO_2 adsorption. The volume of micropores determined from CO_2 measurements was marked as V_{mic}, CO_2.

The X-ray diffraction (XRD) patterns of the carbon from disposable masks were recorded with an X-ray diffractometer (X'Pert–PRO, Panalytical, Almelo, The Netherlands, 2012) using Cu K λ (λ = 0.154 nm) as the radiation source in the 2θ range 10–80° with a step size of 0.026.

Scanning electron microscopy (SEM) images of the surface morphology and feature of the samples were performed on a Zeiss Neon 40 EsB and a Zeiss CrossBeam instrument (Carl Zeiss SMT GmbH, Oberchoken, Germany, 2009) at 5.0 kV equipped with a field emission source.

Raman spectroscopy was used to determine the structure of the carbon skeleton of the obtained carbon materials. Raman analysis was recorded on a InVia Raman Microscope (Renishaw PLC, New Mills, Wotton-under-Edge, UK, 2007) with a laser wavelength of 785 nm. The spectrum obtained in the Raman shift range from 800 cm^{-1} to 2000 cm^{-1} was analysed. After normalizing the maximum of the G peak to 1, the intensity and position of the G and D peaks were read in each spectrum and the ratio of these intensities was determined.

The particle size distribution of the sorbent has been obtained by laser diffractometry using a Mastersizer 3000 granulometer (Malvern Instruments), after the dispersion of powders in water under mechanical agitation of the suspension.

2.3. Adsorption experiments

High purity CO_2 (99.995%) from Air Liquide was applied for CO_2 adsorption measurements. The CO_2 adsorption isotherms were obtained via volumetric apparatus (ASAP 2460). The sample was heated at 250 °C under vacuum for 12 h in order to clean it of gaseous pollutants and water vapor. Measurements of the adsorption were made at 0 °C, 10 °C and 20 °C. A thermostatic bath was used for the tests to keep the sample at the desired experimental temperature.

2.3.1. Fitting of adsorption isotherms

The parameters of the isotherms were determined by nonlinear regression using the solver add-on with the Microsoft Excel spreadsheet for calculations. This method provides an accurate mathematical determination of isotherm parameters using the original form of the isotherm equation. Seven commonly used adsorption isotherms were used to correlate the experimental data, two of which are two-parameter equations: Langmuir, Freundlich and five are three-parameter equations: Sips, Toth, Unilan, Radke-Prausniz, Fritz-Schlunder. According to the model assumptions, the adsorbed quantity is related to the gas pressure following the presented equations in Table 1 [43].

To find the best fitted model, the standard error of each parameter was calculated. In order to evaluate the best fittings of isotherm models to the experimental data, we have applied the sum of the squares of the errors (SSE), which is the most commonly used error function. It is based on the sum of the squares between the measured and calculated values. It is described by the equation [43]:

$$SSE = \sum_{i=1}^{n} (q_{e,o} - \quad q_{e,z})^2$$

were:

$q_{e,o}$ – theoretical adsorption on the sorbent surface calculated on the basis of the model.

$q_{e,z}$ – adsorption on the sorbent surface determined experimentally.

2.3.2. Determination of adsorption heat

The isosteric heat of adsorption is an important parameter in the adsorption processes. The isosteric heat of adsorption as a function of the surface coverage was determined based on the isotherms exhibiting the best fit at different temperatures, utilizing the Clausius-Clapeyron equation:

$$\left(\frac{\partial \ln(p)}{\partial \quad \frac{1}{T}}\right)_{\theta} = \quad \frac{Q_i}{R}$$

where:

Q_i – isosteric heat of adsorption [kJ/mol].

R – gas constant [kJ/mol K].

θ – degree of surface coverage.

T – temperature [K].

In order to determine the isosteric heat of adsorption for the tested materials, the function ln (p) = f (1/T) was used for a given degree of surface coverage in the range from 0.005 to 0.035.

3. Results

3.1. Characteristics of the carbons obtained from protective mask

The XRD method is usually used to identify the crystallographic characteristics of materials. Fig. 1 shows the XRD patterns of the carbons.

The diffraction profiles exhibit only two broad bands around 2θ = 23° and 43°, which are associated with diffraction of the (002) and (10) planes, respectively. The (002) denote the average crystallite thickness and (01) the average graphene sheet diameter [31]. The absence of other signals proved that the activated carbons did not contain any impurities. The broad peaks revealed pre-dominantly an amorphous carbon structure. Similar results were also reported by others [44,45].

The Raman spectra of the carbons in the range of 800–2000 cm^{-1} are shown in Fig. 2.

The Raman spectra of the carbons were dominated by relatively

Table 1
Adsorbed quantity according to the model assumptions.

Isotherm model	Equation	Parameters of the isotherm
Langmuir	$q = \frac{q_{mL} b_L p}{1 + (b_L p)}$	q_{mL} – maximum adsorption on the sorbent surface, [mmol/g] b_L – Langmuir constant, [bar^{-1}]
Freundlich	$q = k_F \; p^{n_F}$	k_F – Freundlich constant, [mmol/g] n_F – heterogeneity factor
Sips	$q = \frac{q_{mS} b_S p^{n_s}}{1 + b_s p^{n_s}}$	q_{mS} – maximum adsorption capacity, [mmol/g] b_S – Sips constant, [bar^{-1}] n_S – heterogeneity factor
Toth	$q = \frac{q_{mT} b_T p}{(1 + (b_T p)^{n_T})^{1/n_T}}$	q_{mT} – maximum adsorption capacity, [mmol/g] b_T – Tooth constant, [bar^{-1}] n_T – heterogeneity factor
Unilan	$q = \frac{q_{mU}}{2s} \ln \left(\frac{1 + b_U \exp^{(S)} p}{1 + b_U \exp^{(-S)} p} \right)$	q_{mU} – maximum adsorption capacity, [mmol/g] b_U –Unilan constant, [bar^{-1}] s – constant depending on the difference between the minimum and maximum adsorption energy
Radke-Prausniz	$q = \frac{q_{mRP} b_{RP} p}{(1 + b_{RP} p)^{n_{RP}}}$	qm_{RP} – maximum adsorption capacity, [mmol/g] b_{RP}, – Radke-Prausnitz constant, [bar^{-1}] n_{RP} –Radke-Prausnitz model exponent
Fritz-Schlunder	$q = \frac{q_{mFS} b_{FS} p}{1 + q_{mFS} p n_{FS}}$	q_{mFS} – maximum adsorption capacity, [mmol/g] b_{FS}, – Fritz-Schlunder constant, [bar^{-1}] n_{FS} –Fritz-Schlunder model exponent

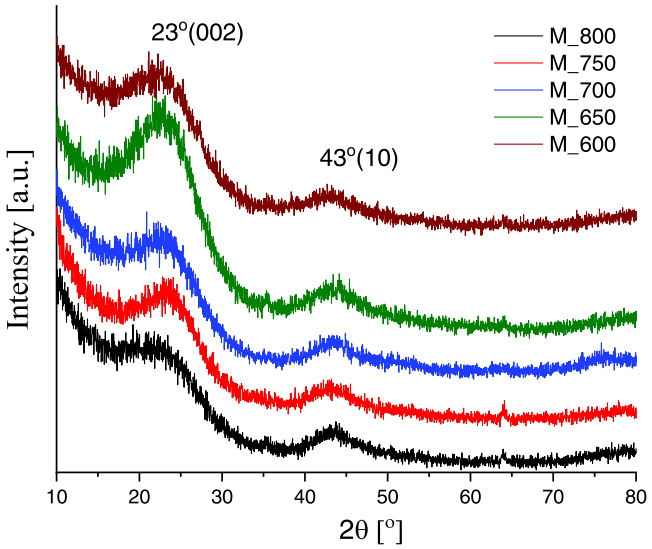

Fig. 1. XRD patterns of carbons from protective masks.

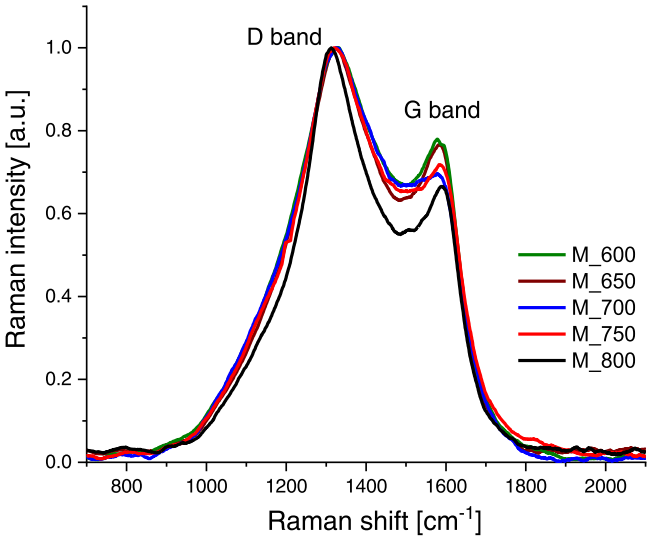

Fig. 2. Raman spectra of carbons from protective masks.

sharp D and G bands. The G band was always present for each carbon material, while with an increasing disorder in the graphite structure, another band appeared, denoted as the D band. The tested carbons obtained from masks had two characteristic bands. In the frequency range, approx. 1600 cm^{-1} (band G) and approx. 1305 cm^{-1} (band D). The G band could be attributed to the in-plane carbon-carbon stretching vibrations of graphite layers, and the D band was thought to have arisen from the structural imperfection of graphite. The intensity D band was proportional to the number of defects [31]. It was noticed that the D band was more intense than the G band, which confirms the poor ordering of the carbon structure and is related to the existence of numerous defects in the structure. Determining the correlation between the location of the G and D bands and their intensity (I_G/I_D) allows to characterize the structural properties of carbon materials. The ratio between the D and G band intensities (I_G/I_D) indicates the graphitization degree of the material. An increase in the I_G/I_D peak intensity ratio indicates a higher degree of carbon graphitization [46].

The values of I_G/I_D ratios obtained from Raman spectroscopy are shown in Table 2.

On the basis of Raman spectra normalized to the G band, I_G/I_D values were estimated. The values of the I_G/I_D ratios for all tested carbons are similar to one another and are in the range from 0.67 to 0.77. An increase in the I_G/I_D ratio indicates a higher ordering associated with the structural disturbance in these carbons. According to values of the I_G/I_D ratio mentioned in Table 2, the M_600 ($I_{G/D} = 0.77$) is more ordered than the M_800 ($I_G/I_D = 0.67$). The influence of the temperature on the I_G/I_D ratio depends on the type of carbon material. Liu et al. [47] produced carbon materials from Huolinhe lignite using two different methods. The I_G/I_D ratio increased with the temperature for the first method and decreased for the second. The influence of KOH: lumpy bracket mass ratio and the temperature on the I_G/I_D ratio was described by Serafin et al. [31]. The values of I_G/I_D for activated biocarbons were in the range of 0.52–0.76. The higher I_G/I_D values were observed in samples obtained at lower and higher temperatures and using the lowest and the highest impregnation ratios of KOH to lumpy bracket. The I_G/I_D

Table 2
Values of I_G/I_D ratios of activated carbons prepared at different temperatures.

Carbon	I_G/I_D
M_600	0.77
M_650	0.76
M_700	0.70
M_750	0.72
M_800	0.67

values decreased in the temperature range of 600–850 °C but for 900 °C IG/ID value was similar to I_G/I_D obtained for 600 °C. The surgical mask waste activated carbons were synthetized at the temperature range of 600–800 °C so the decrease of I_G/I_D values is similar to that described by J. Serafin, et al. [31].

Carbon analysis by Raman spectroscopy confirmed the results of XRD studies. The XRD spectra of activated carbons showed that all of them had a nearly amorphous carbon structure. However, on the basis of Scherrer equation the average crystallite thickness and average graphene sheet diameter can be approximately calculated. For the dimension of turbostratic crystallites perpendicular to the graphene sheets, (002) peak data were used. For the dimension in graphene sheet planes, (10) peak data were used. The brighter the peaks, the lower the values. The values were not calculated. They were determined on the basis of the width of the peaks at half height, standing for the degree of graphitization decreasing with the temperature.

The textural properties of the obtained materials were analysed based on the N_2 adsorption-desorption studies at −196 °C on carbons (Fig. 3).

The N_2 adsorption-desorption isotherms were classified according to the IUPAC as type 1 and 4 isotherms, suggesting that the carbon structure is substantially microporous with the influence of the mesoporous structure [48]. All the isotherms showed a type H3 hysteresis loop. Fig. 4 shows the influence of the activation temperature on the specific surface area, the total pore volume and the volume of micropores determined from N_2 adsorption at −196 °C and CO_2 adsorption at 0 °C for the carbons.

The Brunauer-Emmett-Teller (BET) surface areas shown in Fig. 4a were quite high, and the highest value of 969 m^2/g was obtained for the carbon M_750, the activation temperature of which was 750 °C. The surface areas in order of the largest to the smallest were M_750 > M_700 > M_800 > M_650 and M_600. The total pore volume was calculated assuming the total N_2 under $p / p_0 = 0{,}99$ and it was found that the highest V_{tot} value was also obtained for the carbon M_750 and it was 0.635 cm^3/g (Fig. 4b). As a result of the analysis of Fig. 4c and Fig. 4d it was found that the volume of micropores with diameters in the range 1.4–2 nm and the volume of micropores (except M_700 carbon) showed an increasing trend with increasing activation temperature.

Fig. 5 shows the distribution of pores with diameters of 0.3–1.4 nm determined with the DFT method based on CO_2 adsorption at 0 °C. Fig. 6 presents the same materials and the distribution of pore sizes determined with the DFT method from N_2 adsorption measurements at −196 °C. The pore spreading and porous size distribution of the samples (Figs. 5 and 6) were narrowly distributed within the micro-mesopore range.

Traditionally, the pore size distribution is evaluated from the analysis of nitrogen sorption isotherms measured at 77 K. At such a low temperature diffusion of nitrogen molecules into small micropores is very slow and pores below 1 nm cannot be estimated. This problem can be eliminated by using CO_2 adsorption at 0 °C. The saturation pressure of CO_2 at 0 °C is very high (26141 torr). Therefore low relative pressure measurements necessary for the small micropore analysis are achieved in the range of moderate absolute pressures. At higher temperature and under higher absolute pressures CO_2 molecules can more easily access ultramicropores than N_2 at 77 K in spite of the fact that molecular critical dimensions of both gases are similar.

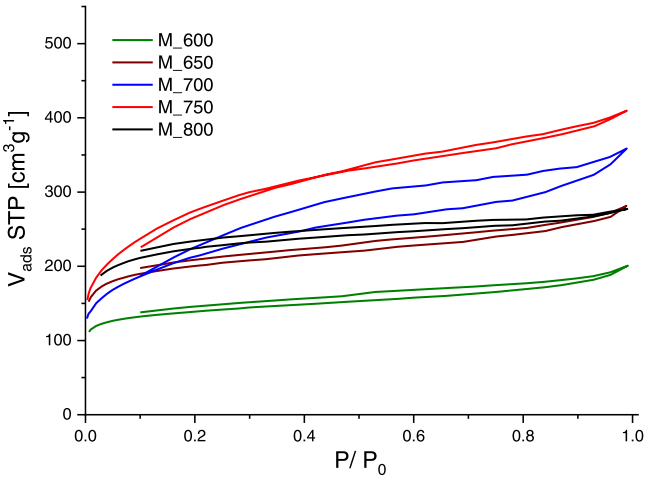

Fig. 3. N_2 adsorption-desorption curves of the samples.

On the basis of nitrogen sorption, pore volume of pores with diameter in the range of about 1.1–100 nm can be estimated. Carbon dioxide sorption gives information concerning the pores with diameter in the range of about 0.3–1.1 nm.

The estimation of small micropores (below 1.2 nm) using CO_2 adsorption at 0 °C is a common method described and has been utilized by many authors [29,49–51].

In Fig. 5 three particularly intense peaks can be observed at pore diameters of 0.35–0.4 nm, 0.4–0.7 nm, and 0.7–1 nm. These peaks occurred in all carbons regardless of the activation temperature. They show the share of narrow micropores in the activated carbons, the largest share of which was observed in the sample carbonized at the temperature of 800 °C. The micropore volume for sample M_800 determined using carbon dioxide was 0.327 cm^3/g. The curves presenting the pore size distribution of narrow micropores seemed similar but the total narrow pores volumes were different. Moreover the big differences were observed for the pores with the diameter of about 0.8 nm (0.7–1 nm).

The analysed activated carbons in their structure, apart from narrow micropores determined with the use of CO_2 at 0 °C, also contained micropores with a size of 1.4–2 nm and mesopores as shown in.

Fig. 6. A significant increase in mesopores in the pore range from 2 nm to 5 nm was found for samples M_700 and M_750 compared to other materials where such a large increase in the proportion of mesopores was not observed. The participation of mesopores in the tested materials is visible up to the pore width range of 12 nm, as evidenced by the data presented in Fig. 6.

Particle size for activated carbons was measured. Fig. 7 shows the particle size distribution of activated carbons.

Based on the particle size distribution, activated carbons thus produced were mostly 20–60 μm in diameter with more than 80% of particles of size less than 60 μm. The finer the particle size of an activated carbon, the better the access to the surface area [52].

The above results showed that the temperature of the activation process had a strong effect on the texture of carbons. The carbons with KOH as the activator showed higher microporosity content and higher surface area due to intercalation of active K molecules with carbon lattices and carbon matrix than when using other activators [53–56]. Fig. 8 shows pictures taken with a scanning electron microscope at a magnification of 9.000 magnification in order to observe the surface topography of the materials.

According to the SEM micrograph, the ACs have a highly heterogeneous surface and a wider irregularity. No difference in the morphology of activated carbons prepared at different temperatures was observed. They seemed to be very similar.

The TEM pictures were very similar (Fig. 9) and we were not able to judge on the basis of TEM investigation which activated carbon was more porous. The nitrogen adsorption (Fig. 4) gave more information about porosity. However, TEM investigations confirmed the porosity of the samples.

3.2. CO_2 adsorption studies

Fig. 10 shows the results of CO_2 adsorption studies. The data presented in Fig. 10 can be used to compare activated carbon samples that were tested up to a pressure of 1 bar at temperatures of 0 °C, 10 °C and

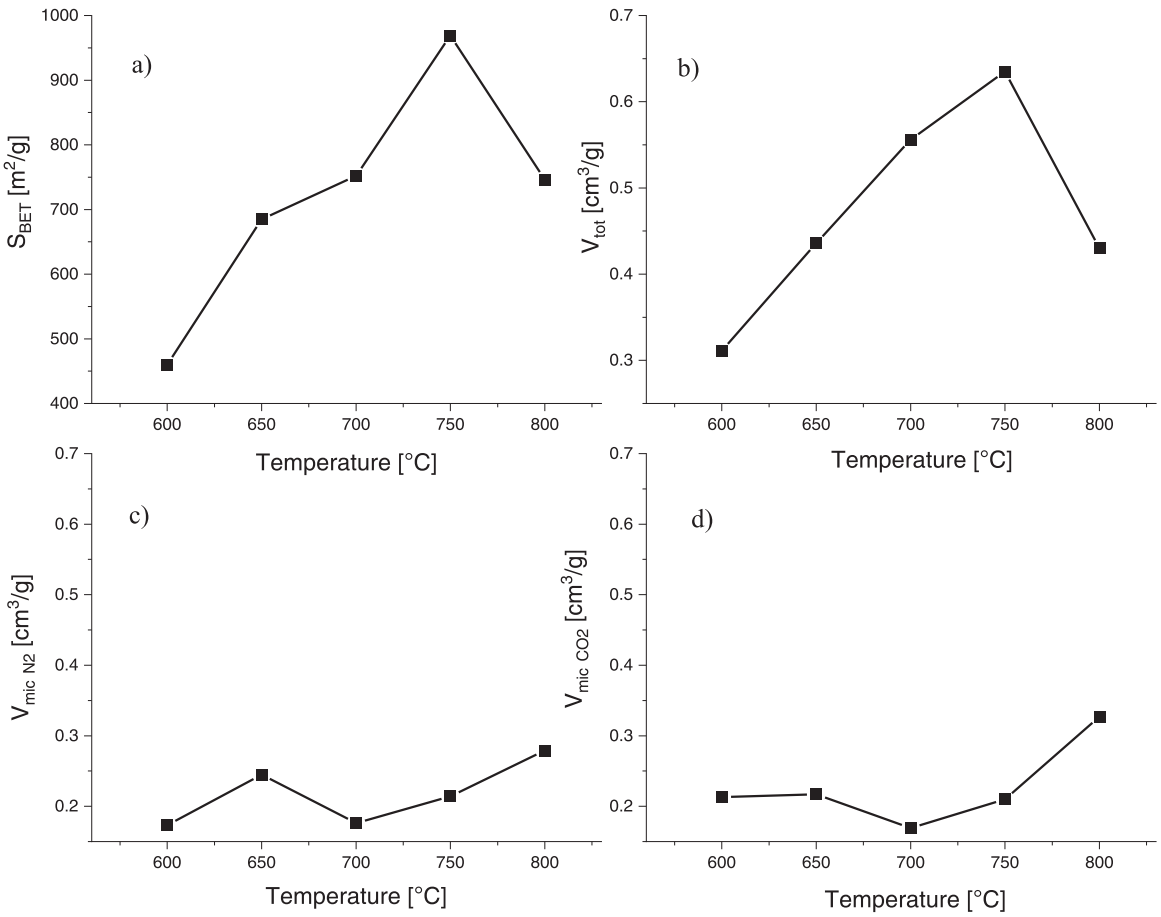

Fig. 4. Relationship between a) specific surface area (S_{BET}), b) total pore volume (V_{tot}), c) micropore volume ($V_{mic\ N2}$), d) micropore volume ($V_{mic\ CO2}$) and the activation temperature of the carbons.

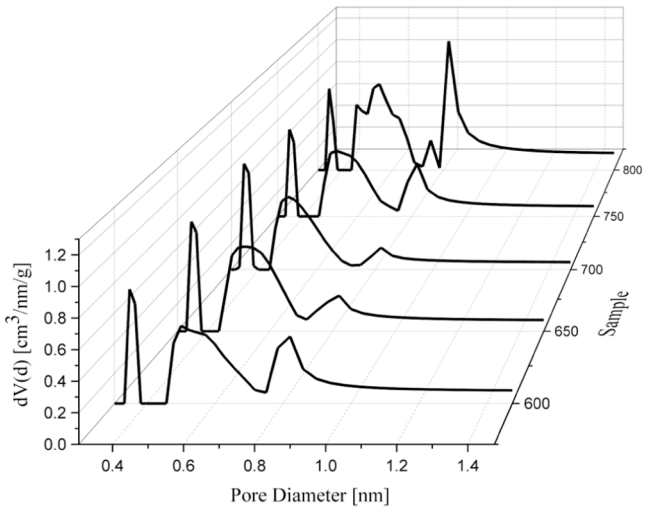

Fig. 5. Pore size distribution determined with the DFT method on the basis of CO_2 adsorption isotherms.

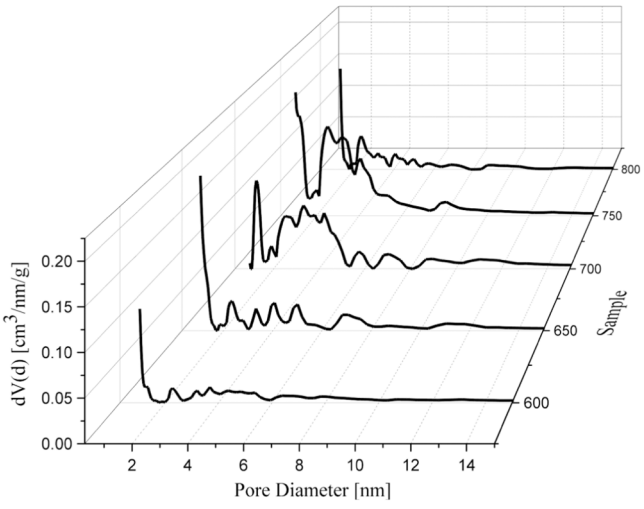

Fig. 6. Carbon pore size distribution determined with the DFT method on the basis of N_2 adsorption isotherms.

20 °C.

Changing the process temperature affected the amount adsorbed in each sample. For all carbons, the adsorption capacity increased with increasing pressure and decreased with increasing temperature, indicating the adsorption was exothermic in behavior which was expected for physical adsorption [57]. The lower CO_2 adsorption capacity resulted mainly from the reduction of interaction forces and binding forces between the adsorbate and the adsorbent [58]. Moreover, this tendency confirms an increase in the energy of CO_2 molecules at a higher temperature, which leads to lower adsorption of CO_2 by AC [59]. All CO_2 isotherms conform to the type I isotherm according to the IUPAC isotherm classification [60]. For carbons prepared from masks, CO_2 adsorption isotherms in the range temperatures of 0–20 °C show a similar course, rapidly rising at low pressures and slowing at higher

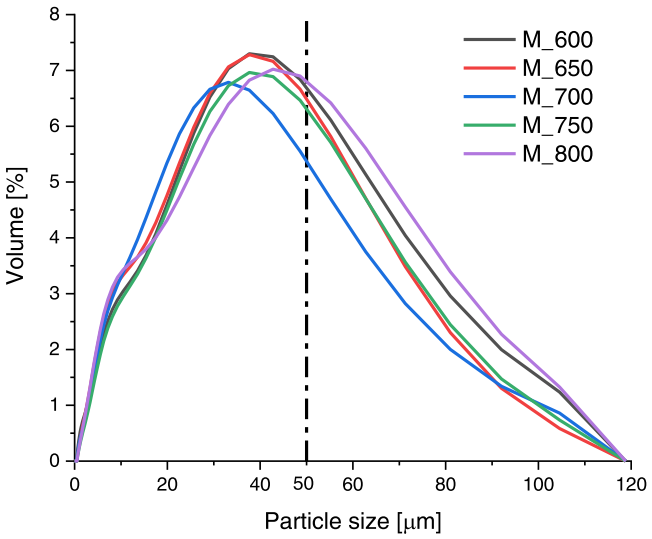

Fig. 7. Particle size distribution of activated carbons.

pressures. These isothermal similarities indicate that the adsorption mechanism was the same for all tested activated carbon samples. Temperature change affected the amount adsorbed in each sample, and CO_2 uptake decreased with increasing temperature. On the basis of Fig. 10, it was found that the carbon synthesized at 800 °C had the highest CO_2 adsorption capacity at a pressure of 1 bar and a temperature of 0 °C. This adsorption capacity was 3.91 mmol/g at 0 °C, whereas at 10 °C it was 3.23 mmol/g, and at 20 °C it was 2.61 mmol/g. The CO_2 adsorption increased with the temperature of the carbonization but at the temperature of 850 °C the yield of the carbonization was very low and we could not produce activated carbons at temperatures higher than 800 °C.

The Table 3 summarizes the results of CO_2 adsorption on activated carbons produced from various carbon precursors. Although the result we obtained for the CO_2 adsorption was not the best, it could still be competitive compared to other materials.

In order to analyse how the textural parameters influence the adsorption of CO_2 at 0 °C, 10 °C and 20 °C at 1 bar, the relationships between them and CO_2 sorption were investigated (Fig. 11).

Fig. 11 shows the effect of the specific surface area (Fig. 11a), the total pore volume (Fig. 11b), the micropore volume determined from the N_2 measurements at −196 °C (Fig. 11c) the volume of the micropores

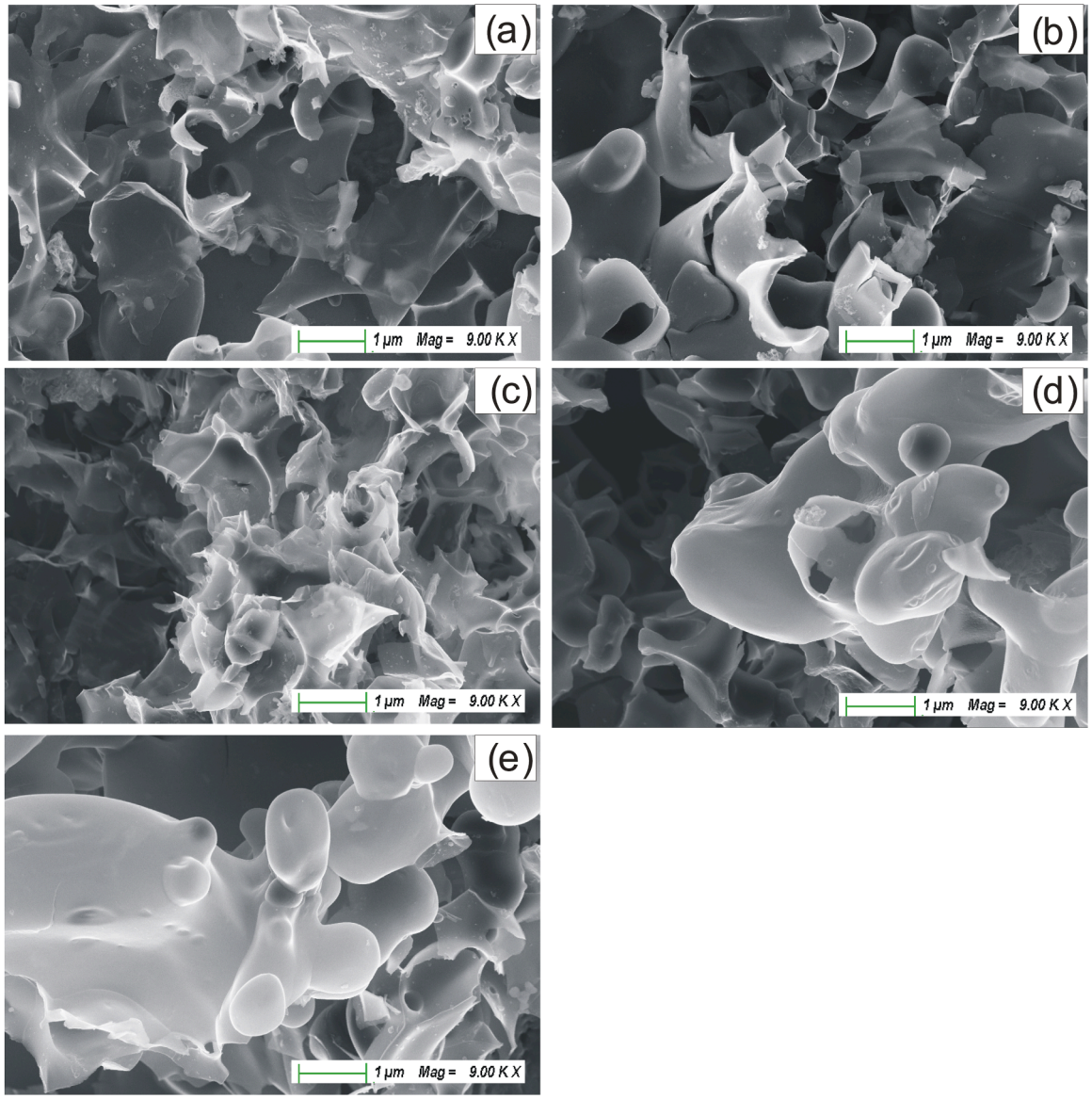

Fig. 8. SEM micrographs of the carbons from protective masks (a) M_600 (b) M_650 (c) M_700 (d) M_750 (e) M_800.

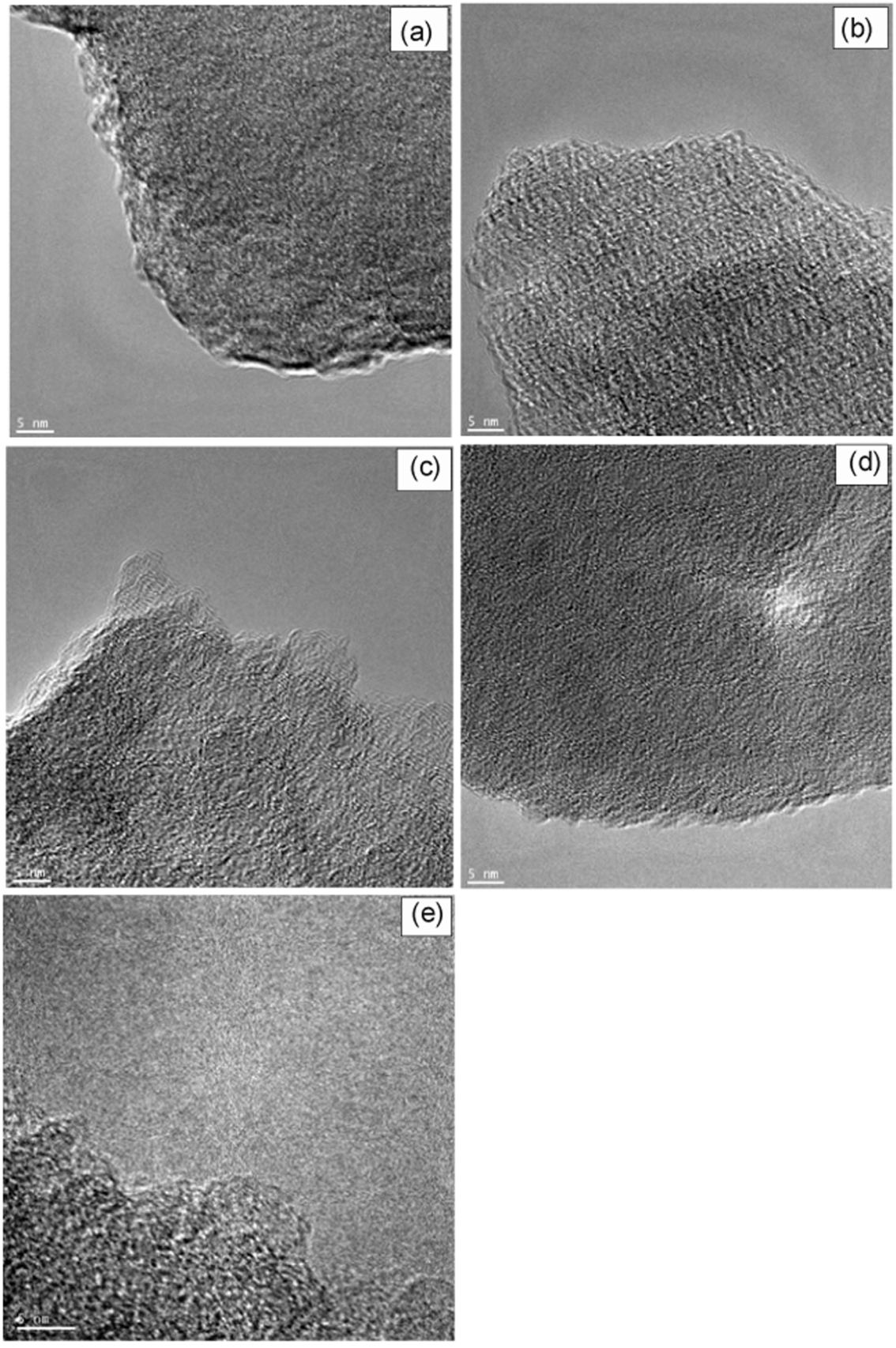

Fig. 9. TEM micrographs of the carbons from protective masks (a) M_600 (b) M_650 (c) M_700 (d) M_750 (e) M_800.

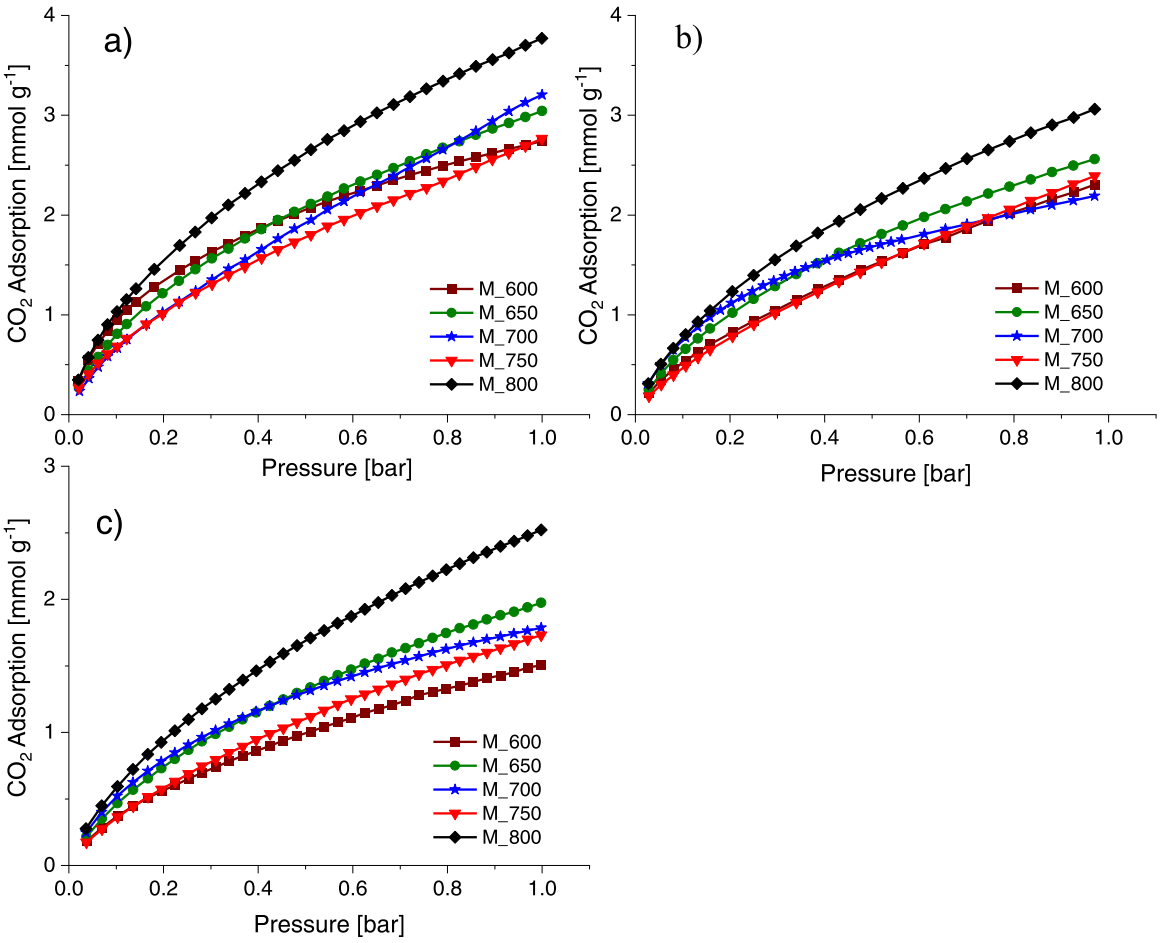

Fig. 10. CO_2 adsorption at temperatures of (a) 0 °C, (b) 10 °C and (c) 20 °C. The symbols represent experimental data. The lines are based on the Sips model.

Table 3
CO_2 adsorption of various carbons at 1 bar and 0 °C.

Material	CO_2 adsorption at 0 °C [mmol/g]	Ref.
organic framework polymers with intrinsic microporosity	2.9	[61]
activated carbon xerogels	4.9	[62]
Mg and N-doped mesoporous carbon	3.6	[63]
waste wool-derived N-doped hierarchical porous carbon	3.7	[64]
fruit waste	7.2	[65]
activated carbon monoliths	2.7	[66]
activated carbon from waste CDs	4.3	[67]
ordered mesoporous carbon	3.0	[68]
graphene aerogels	2.5	[69]
lignocellulose	5.2	[70]
pine cones	3.0	[71]
M_800	3.9	this work

determined from CO_2 measurements at 0 °C (Fig. 11d) for CO_2 adsorption. The coefficient of determination R^2 is the proportion of the variance in the dependent variable that is predictable from the independent variable. An R^2 of 1 means the dependent variable can be predicted without error from the independent variable. A low R^2 value indicates no dependency between the variables. On the basis of the R^2 values presented in Fig. 11 conclusions were drawn about the influence of S_{BET}, V_{tot}, $V_{mic\ N2}$, $V_{mic\ CO2}$ on CO_2 adsorption.

There was no correlation between CO_2 uptake and the specific surface area and the total pore volume. Moreover, the relevant dependence between CO_2 adsorption and micropore volume ($V_{mic\ N2}$) was not evidenced. However, the best correlation was obtained between CO_2 adsorption and the volume of micropores determined from CO_2 measurements at 0 °C. Based on Fig. 5, it was concluded that the carbonaceous materials contained micropores in the pore range from 0.4 to 1 nm which were determined on the basis of CO_2 adsorption measurements. Thus, the high CO_2 uptake was conditioned by the micropore with the diameter from above-mentioned range.

The effective micropores were mainly responsible for CO_2 adsorption on the well-developed activated carbons via a micropore filling mechanism [72]. This was due to the fact that CO_2 particles were captured by micropores [73] and the amount of CO_2 adsorbed on activated carbons related primarily to narrow micropore volumes [74]. Although the M_750 carbon showed a more developed specific surface than other samples, it did not have the highest CO_2 adsorption capacity compared to other carbons. The sample M_800, which showed the greatest development of micropores volume in the range 0.4–1 nm, also showed the greatest adsorption of CO_2 at temperatures 0, 10 and 20 °C (Fig. 10). On the basis of Figs. 5 and 11, the assumption was made that pores with the diameter of about 0.8 nm (0.7–1 nm) are the most important for CO_2 adsorption at the pressure of 1 bar.

The correlation of textural parameters and CO_2 adsorption at 1 bar was investigated by other authors. Martín et al. [49] showed that CO_2 adsorption at 1 bar and the temperature of 25 °C correlated well with narrow microporosity estimated using CO_2 adsorption at 0 °C. Martín-Martínez et al. [75] showed that only pore sizes less than 5 times that of the molecular size of the adsorbate were effective for gas adsorption at atmospheric pressure. In the particular case of CO_2, it has been demonstrated empirically as well as by mathematical simulation, using

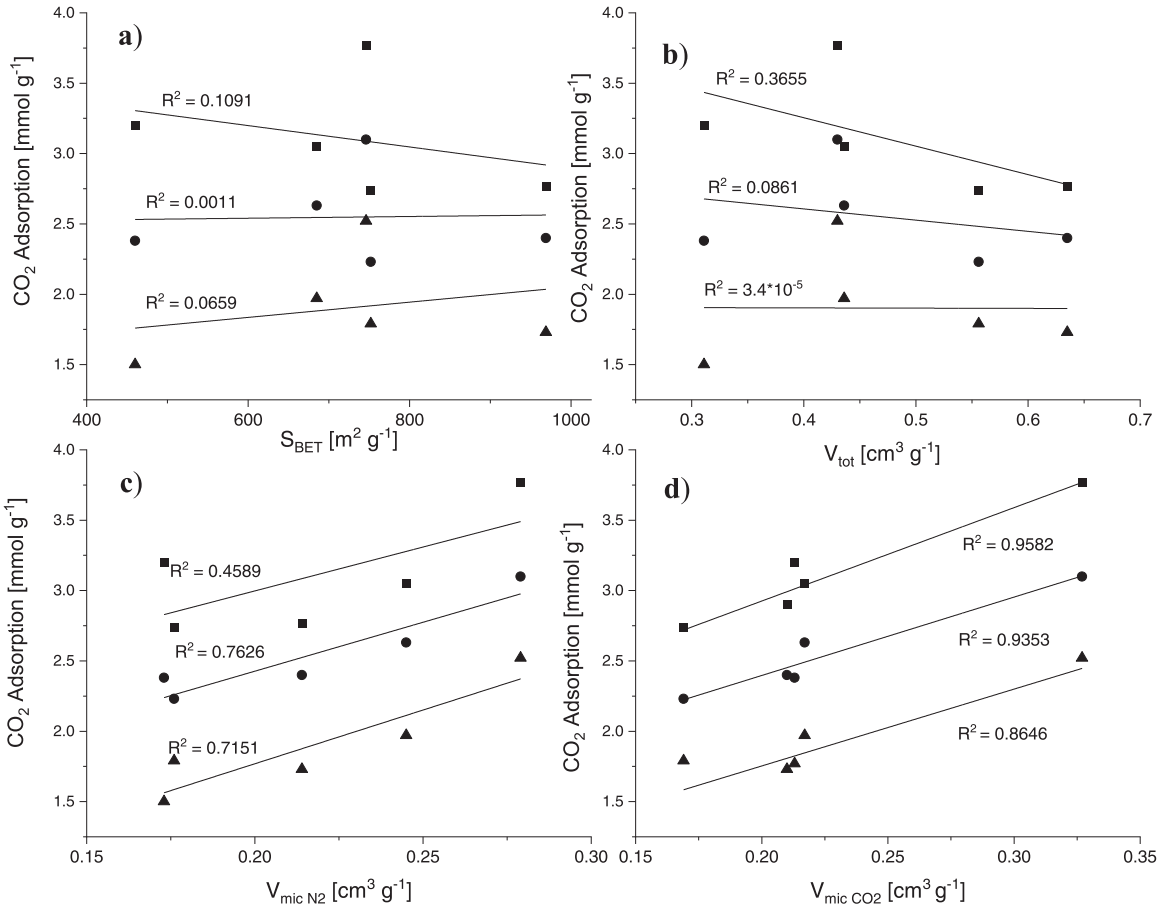

Fig. 11. The CO_2 adsorption at the pressure of 1 bar and at ■ 0 °C, •10 °C and ▲20 °C temperature as a function of (a) S_{BET} (b) V_{tot} (c) $V_{mic\ N2}$ (d) $V_{mic\ CO2}$.

grand canonical Monte Carlo (GCMC) and the nonlocal density functional theory [76] that only pores of less than 1 nm can be effective for CO_2 adsorption at atmospheric pressure. Wickramaratne et al. [50], Grundy et al. [29], Li et al. [51] proved that CO_2 adsorption at 0 °C and 1 bar depended on the micropore smaller than 1 nm. These authors utilized CO_2 as the adsorbate, temperature of 0 °C and p/p0 up to 0.3 for small micropore volume and distribution.

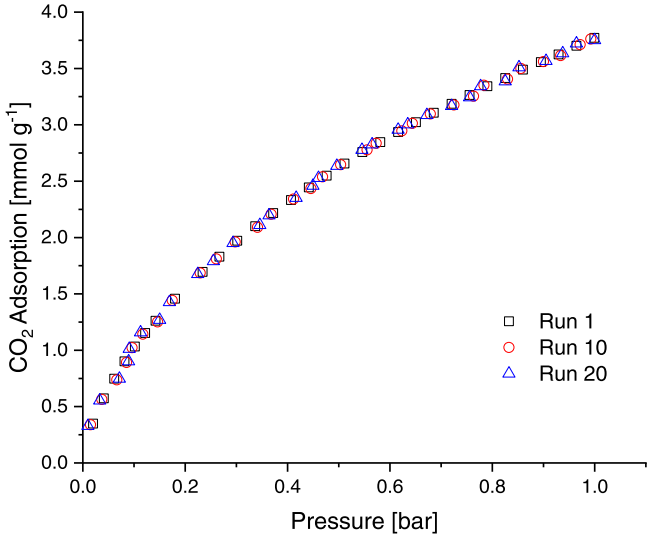

Fig. 12. Multi-cycle CO_2 adsorption isotherms for M_800 at 0 °C, 1st, 10th, 20th adsorption isotherm.

The re-usability of M_800 as a CO_2 sorbent was examined. Twenty adsorption–desorption cycles at a temperature of 0 °C were performed. Fig. 12 presents 1st, 10th, 20th adsorption isotherms. No changes in the CO_2 adsorption after twenty cycles were found. The highest standard deviation was equal to 0.06. The reproducibility and repeatability of CO_2 adsorption on M_800 activated carbon was proved. M_800 was a stable CO_2 sorbent and it could be regenerated without any loss of its CO_2 sorption capacity.

3.2.1. *Fitting results*

The experimental values of CO_2 adsorption isotherms presented in Fig. 10 were analysed using seven equations: Langmuir, Freundlich, Sips, Toth, Unilan, Radke-Prausniz and Fritz-Schlunder. Table 4 presents values of the SSE error of CO_2 adsorption isotherms for each analysed model. The lowest SSE values were found to determine which model was the best. Based on the squares of the errors (SSE), it was found that the Sips equation gave the highest accuracy of fitting to the experimental data. Using the Sips model, the lowest SSE values were obtained for each CO_2 adsorption isotherm at temperatures of 0 °C, 10 °C and 20 °C of the tested carbons, as shown in Table 4.

Table 5 presents the determined parameters of the Sips isotherm for different temperatures of the CO_2 adsorption process.

The Sips model was the most suitable for fitting CO_2 adsorption on carbons from waste face masks. The Sips isotherm is a combination of the Langmuir and Freundlich isotherms. The difference between the Sips and the Langmuir equation is the heterogeneity factor n_s, usually lower than 1. The smaller the value of this parameter, the more heterogeneous the adsorbent surface. If n_s is equal to 1, the Sips equation is reduced to the Langmuir equation and the surface is homogeneous. The values of n_s in the temperature from 0 to 20 °C were in the range of 0.663–0.792.

Table 4
Values of the SSE error of CO_2 adsorption isotherms for each analysed model.

Carbon	Freundlich	Langmuir	Sips	Toth	Unilan	Fritz-Schlunder	Radke-Prausnitz
	Temperature 0 °C						
M_600	0.04745	0.08763	0.00024	0.00075	0.02029	0.00031	0.00123
M_650	0.01890	0.18456	0.00100	0.00242	0.02721	0.00203	0.01890
M_700	0.02415	0.24366	0.01421	0.21789	0.06337	0.02415	0.02415
M_750	0.01050	0.25595	0.00906	0.03010	0.05720	0.01060	0.01052
M_800	0.03635	0.28413	0.00100	0.01247	0.05731	0.03635	0.03635
	Temperature 10 °C						
M_600	0.00079	0.07987	0.00064	0.00329	0.03918	0.00077	0.00078
M_650	0.01872	0.06705	0.00015	0.00022	0.01884	0.00059	0.00119
M_700	0.06943	0.08076	0.00372	0.00618	0.01037	0.00435	0.06942
M_750	0.07625	0.05649	0.00020	0.00313	0.02918	0.00046	0.00046
M_800	0.01992	0.11595	0.00014	0.00065	0.03355	0.00058	0.00058
	Temperature 20 °C						
M_600	0.00186	0.03444	0.00083	0.01141	0.01934	0.00096	0.00097
M_650	0.01212	0.03312	0.00028	0.00031	0.01346	0.00035	0.00037
M_700	0.02795	0.02999	0.00010	0.00111	0.00482	0.00039	0.00031
M_750	0.00365	0.02225	0.00037	0.00314	0.01289	0.00069	0.00079
M_800	0.01517	0.05871	0.00012	0.00114	0.02563	0.00043	0.00139

Table 5
Sips isotherm parameters.

Isotherm parameters	Temperature of adsorption CO_2 [°C]	Carbon				
		M_600	M_650	M_700	M_750	M_800
q_{ms}	0	12.185	14.319	6.857	10.172	15.016
[mmol/g]	10	10.225	9.198	4.220	9.831	12.577
	20	6.140	6.994	3.974	9.794	9.909
b_s	0	0.788	0.393	0.861	0.578	0.335
[bar^{-1}]	10	0.114	0.374	0.817	0.437	0.329
	20	0.142	0.269	0.805	0.422	0.342
n_s	0	0.655	0.682	0.763	0.706	0.699
	10	0.663	0.703	0.771	0.731	0.701
	20	0.668	0.725	0.792	0.789	0.736

This proves the heterogeneity of the activated carbon surface.

Parameters in the Sips equation such as b_s n_s and q_{ms} are temperature-dependent:

$$b_s = b_0 \bullet \exp\left(\frac{Q}{R \bullet T_0}\right) \bullet \left(\frac{T_0}{T} - 1\right); n_s = n_0 + \alpha\left(1 - \frac{T_0}{T}\right);$$

$$q_{ms} = qm_0 \bullet \exp\left(\chi\left(1 - \frac{T}{T_0}\right)\right)$$

In the above equations, b_0 – adsorption affinity, n_0 – heterogeneity coefficient, q_{m0} - maximum adsorption capacity, χ and α are constants, R is the gas constant and T_0 is the reference temperature, which was assumed in the study to be 0 °C (the lowest process temperature), and Q is the isosteric heat of adsorption with the coverage degree tending to zero. These parameters were determined using graphs showing the dependencies of ln (b_s) from 1/T, ns from 1/T and ln (q_{ms}) from T. The exemplary graphs for the M_750 carbon are shown in Fig. 13.

High values of R^2 were obtained, which proves a good fit of these dependencies to the linear function. This confirms the correctness of the performed calculations related to the determination of the parameters of the Sips model at the tested temperatures of CO_2 adsorption. The determined temperature-dependent parameters in the Sips equation are presented in Table 6.

3.2.2. Heat of adsorption

The isosteric heat of adsorption is important to characterize the interaction between the adsorbent and the adsorbate. A higher value of isosteric heat of adsorption proves a stronger interaction between carbon dioxide and the tested carbons. The isosteric heat of adsorption was calculated from the experimental data obtained at 0–20 °C using the Sips temperature equations and the linear form of Clausius-Clapeyron equation

$$\ln(p)_\theta = -\frac{Q_i}{R}\frac{1}{T} + C$$

where:

C is a constant.
θ – surface coverage.
Q_i – isosteric heat of adsorption [J mol^{-1}].
R – ideal gas constant [m^3 Pa K^{-1} mol^{-1}].
T – temperature [K].

First, the experimental isotherms were fitted to Sips equations to calculate numerically θ for a given p at different temperatures. The isosteres were plotted in coordinates ln(p) vs. 1/T for seven surface coverage (θ = 0.005, 0.010, 0.015, 0.020, 0.025, 0.30, 0.035) and presented at the Fig. 14. The isosteres gave the information about the energetic homogeneity of the surface in question. At each given θ, the isostere plot of (ln p) as function of (1/T) matches with the linear form of Clausius-Clapeyron equation. Therefore, the isosteric head of adsorption values were calculated from the slopes of the isostere plot:

$$Q_i = -\text{ slope} \bullet R$$

The linear fit of all f(1/T)= ln(p) showed that the derivative $\left(\frac{\partial \ln(p)}{\partial \frac{1}{T}}\right)_\theta$ was independent from the temperature but the influence of the surface coverage was observed in the temperature range of 0–20 °C. This indicates the homogeneity of the adsorbent surface [54].

Fig. 15 shows the determined values of the isosteric heat of CO_2 adsorption on the carbon as a function of the degree of surface coverage.

The determined values of the isosteric heat of adsorption for carbons did not show any significant variability and ranged from 19 to 25 kJ/mol. These values strongly confirm the physical nature of CO_2 sorption on the carbon materials from the masks. As the degree of surface coverage increased, the isosteric heat of adsorption decreased. The isosteric heat of adsorption decreased as there was less and less interaction of CO_2 with the material. In a common adsorption process, the adsorptive becomes attached to the surface of the adsorbent and forms the adsorbate. If the heat of adsorption of the first layer is comparable, usually slightly lower than the heat of the subsequent layers, it mean that physical sorption took place. Therefore, we can hypothesize about physisorption of CO_2 on activated carbons produced from face mask. The values of isosteric adsorption heat determined on the basis of Clausius-Clapeyron equation are consistent with the values of the heat

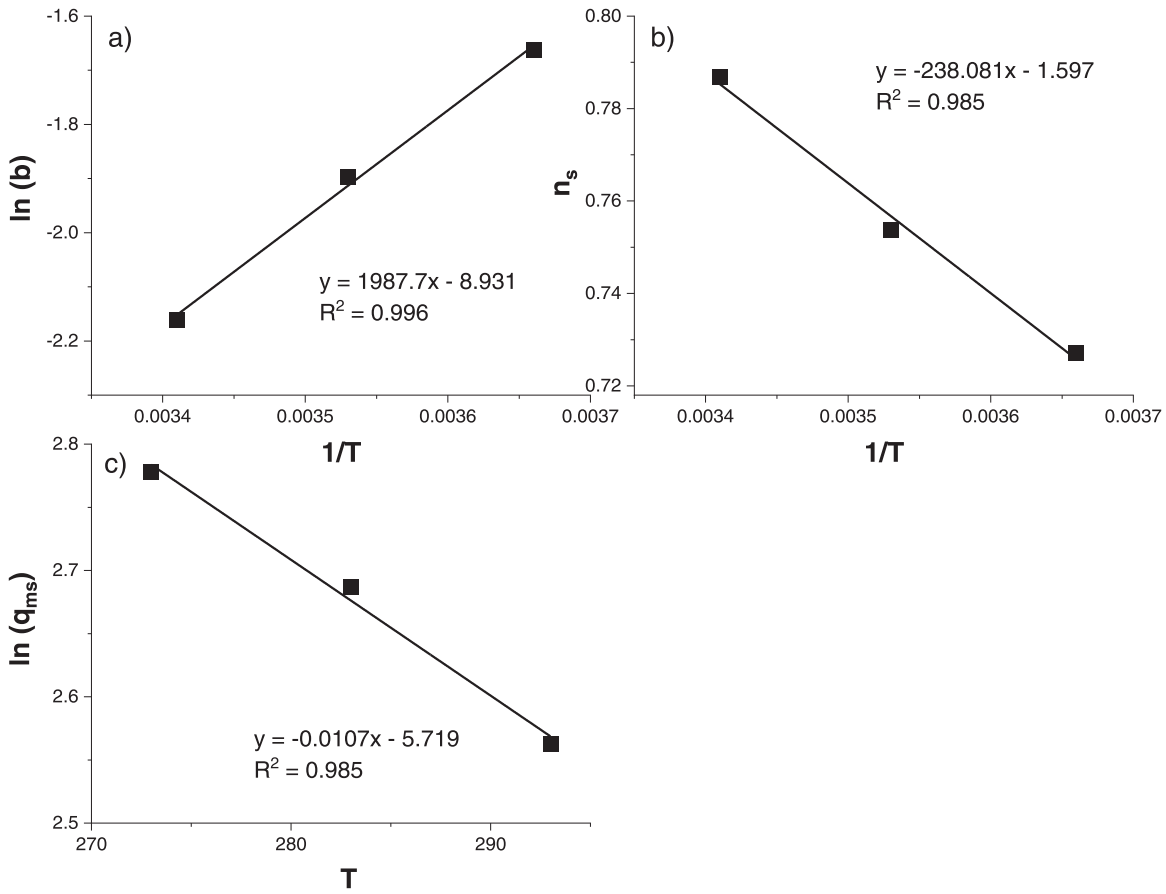

Fig. 13. Dependence of a) the natural logarithm of the bs coefficient of the reciprocal of temperature; b) the ns coefficient of the reciprocal of temperature; c) the natural logarithm of q_{ms} from temperature.

Table 6
The parameters of temperature dependent Sips equations.

Carbon	b_0 [bar^{-1}]	Q [kJ/mol]	n_0	α	χ	q_{mo} [mmol/g]
M_600	0.15	26	0.66	0.39	1.35	4.97
M_650	0.13	27	0.68	0.37	1.68	5.88
M_700	0.16	27	0.76	0.41	1.44	5.92
M_750	0.18	28	0.70	0.42	1.51	4.99
M_800	0.20	29	0.69	0.38	1.45	6.21

determined with the degree of coverage approaching zero (Table 6). The obtained results are in good agreement with the results obtained by other researchers [77,78].

The isosteric heats of CO_2 adsorption are very similar for all activated carbons. The lowest values were obtained for M_600 and they ranged from 22 to 19 kJ/mol. The highest values of isosteric heats of CO_2 adsorption were observed for M_800 and they ranged from 25 to 21 kJ/mol.

The higher heat for M_800 proved the higher interaction between CO_2 and surface of this material. The isosteric heat of adsorption becomes constant at high coverage for M_800 suggesting a uniform CO_2 adsorption on this material from surface coverage of 0.02.

Selectivity adsorption of CO_2 over N_2 is a significant factor that ought to be taken into account in evaluation of the sorbents for CO_2 adsorption. Therefore, nitrogen adsorption measurement at 20 °C up to a pressure of 1 bar was performed for the sample M_800 which had the best CO_2 adsorption.

The ideal adsorbed solution theory (IAST) proposed by Myers and Prausnitz [79] is widely used for predicting the adsorption selectivity and mixed-gas adsorption isotherms from pure-component isotherms with a rational accuracy for various systems. In this work, IAST was employed to predict selectivity of CO_2 over N_2 using single adsorption isotherms of these gasses for equimolar CO_2 and N_2 binary mixture (S_{EQM}) according to the following equation [80]:

$$S_{EQM} = \frac{q_{CO_{2(p)}}}{q_{N_{2(p)}}}$$

where: $q_{i(p)}$ is the adsorption capacity [mmol/g] at the same partial pressure p of CO_2 and N_2.

Typical flue gas composition in vol% is: 67–72% nitrogen, 8–10% carbon dioxide, 18–20% water steam, 2–3% oxygen for natural gas-fired power plants and 72–77% nitrogen, 12–14% carbon dioxide, 8–10% water steam, 3–5% oxygen for coal-fired boilers [56].

Selectivity for flue gas composition 15% CO_2 and 85% N_2 (S_{FG}) was calculated also on the basis of IAST method using the below equation [81]:

$$S_{FG} = \frac{q_{CO_2@0.15bar}}{q_{N_2@0.85bar}} \times \frac{0.85}{0.15}$$

where:

$q_{i@jbar}$ is the adsorption capacity [mmol/g] of CO_2 and N_2 at the partial pressure of 0.15 and 0.85 respectively.

The selectivity was also calculated using the ratios of the Henry's law constants (S_H). The Henry's law constants were estimated from the initial slopes of CO_2 (I_{CO_2}) and N_2 (I_{N_2}) adsorption isotherms according to the equation [82]:

$$S_H = \frac{I_{CO_2}}{I_{N_2}}$$

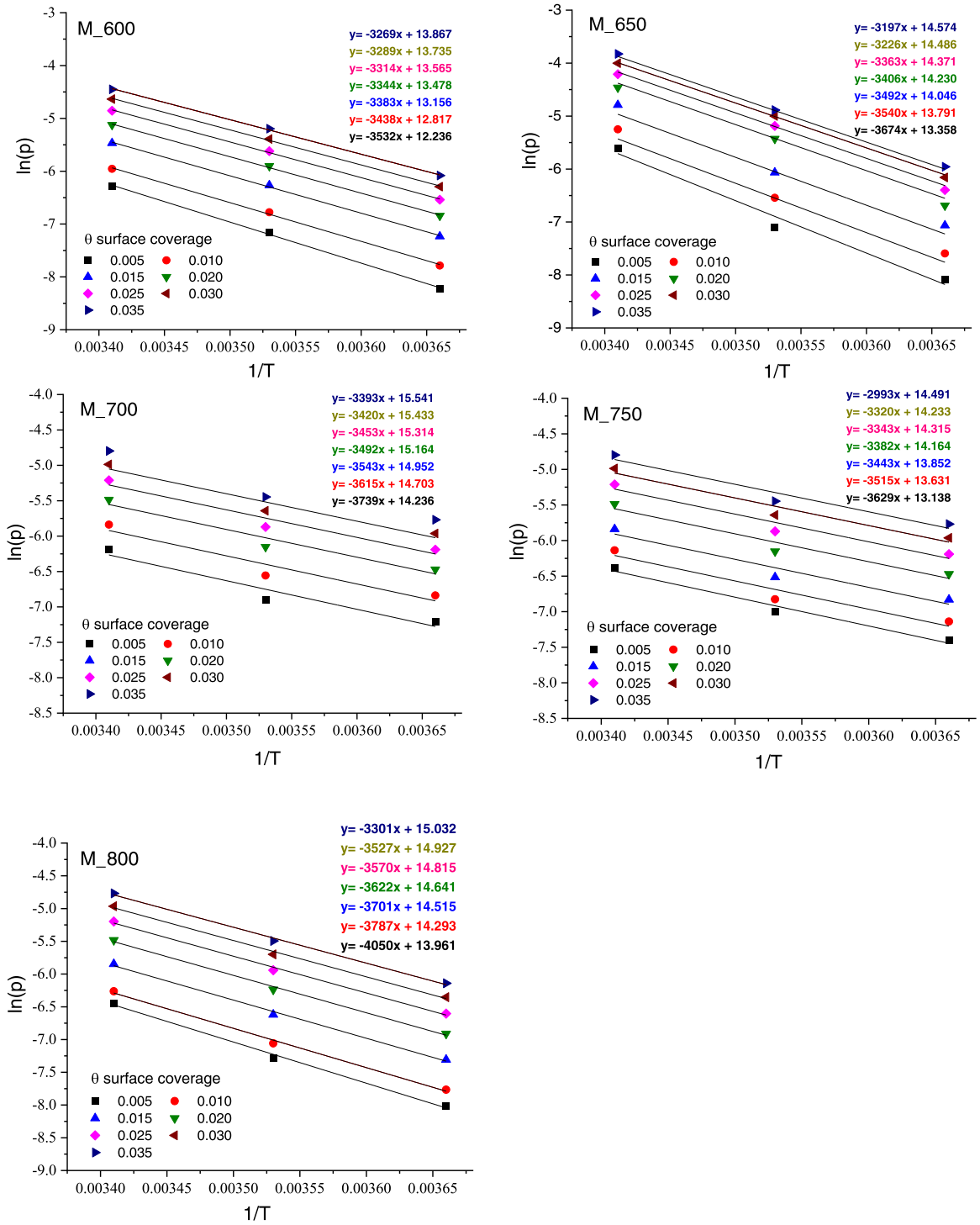

Fig. 14. Adsorption isosteres at different surface coverage (0.005–0.035).

Selectivity calculated using single component gas adsorption capacity for equimolar CO_2 and N_2 binary mixture is presented in Fig. 16.

The CO_2/N_2 selectivity ratio for the M_800 carbon decreased to a pressure of about 0.2 bar. The highest CO_2/N_2 selectivity coefficient at 0.001 bar was 68, while with increasing pressure, the value of the selectivity coefficient decreased, reaching the value of 15 for a pressure of 1 bar. A similar tendency in the CO_2/N_2 selectivity ratio was noted by Serafin et al. [56].

Table 7 presents the selectivity of CO_2 over N_2 of activated carbons prepared from different precursors calculated using different methods at the temperature of 25 °C. The investigations presented in this study were performed at the temperature slightly lower (20 °C) but there is no much work about selectivity of CO_2 over N_2 and the most of them were performed at 25 °C.

Most activated carbons presented in Table 7 had lower selectivity for CO_2 over N_2 than the M_800 produced from surgical mask waste. The high selectivity is one of the important requirements of a good adsorbent.

4. Cost of producing activated carbon

The economic evaluation of production of activated carbons from

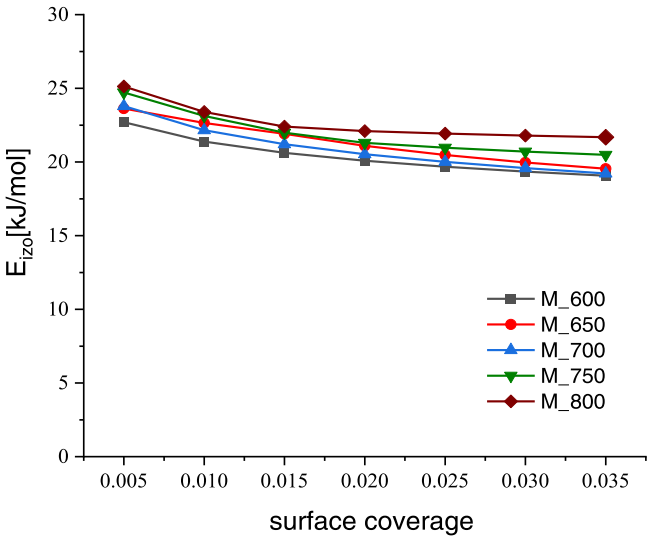

Fig. 15. The isosteric heat of CO_2 adsorption as a function of surface coverage of carbons.

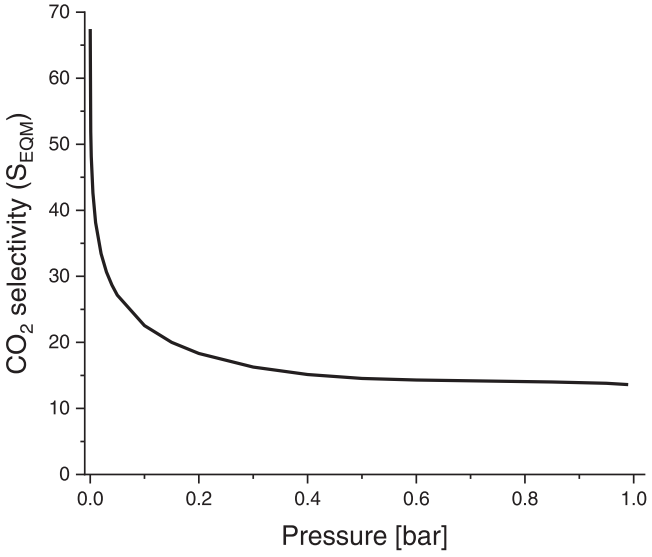

Fig. 16. Selectivity of CO_2 over N_2 calculated using single component gas adsorption capacity for equimolar CO_2 and N_2 binary mixture as a function of total pressure for M_800.

Table 7
Comparison of selectivity of CO_2 over N_2 calculated using different methods at 25 °C on activated carbons obtained from different precursors.

Precursors	S_{EQM} (at 1 bar)	S_{FG}	S_H	Ref.
Polyindole		31.8	58.9	[83]
Polyindole-modified graphene oxide sheets		39.7	23	[84]
Olive stones		15.2		[85]
Eucalyptus saw dust	5.4			[37]
Fungi			18.5	[86]
Petroleum pitch	2.4			[87]
Petroleum pitch-phenolic resin			15.4	[88]
Polyaniline	8.42			[89]
Chitosan	21			[90]
Crab shell		23.1		[72]
Algae-glucose		17.3		[91]
Surgical mask waste (at 20 °C)	15	27.9	23.7	This study

surgical masks was performed. Activated carbons from surgical masks were produced with chemical activation with potassium hydroxide. The preparation process is described in Section 2.1. On the basis of the obtained data, we made calculations on an industrial scale of production. The initial input of 10,000 kg delivered daily was assumed. The yield of carbon after carbonization was 40% (4000 kg), after cleaning and drying, the final yield was 35% (3500 kg).

The first stage of activated carbon preparation from disposable face masks is treatment with a saturated KOH solution for 3 h. Is well known that weak alkali solutions inactivate viruses. Jeong et al. [92] proved that influenza A virus H1N1 was completely inactivated within 1 min of 0.1 mol/dm^3 NaOH treatment. The coronavirus and any other viruses will be completely destroyed in a saturated KOH solution in several seconds. The people who will put the surgical mask waste into the KOH solution should wear personal protective equipment (PPE) for the health workforce during COVID-19 (surgical masks, particulate filter respirators (such as P2 or N95), gloves, goggles, glasses, face shields, gowns and aprons). The cost of PPE is relatively low and there is no need to take it into consideration.

Surgical masks are cut into small pieces with a diameter of 10 mm using an 11 kW cutting machine. After grinding, the material is activated (3 h) with KOH in the ratio of 1 kg of material to 1 l of KOH at room temperature. A 4000 l storage tank is used for the activation process. The material is then transferred to the hopper of a 0.97 × 6.1 m rotary dryer using the parameters established by McCabe et. al. [93]. To prevent rusting and reacting with potassium hydroxide, use a stainless steel dryer. The next step is to transfer the material to a 5 × 1.5 × 0.2 m horizontal tube furnace and carbonize it for 1 h at 700 °C under nitrogen atmosphere. After carbonization, the material should be transferred to a rotary cooler, which is suitable for operation at high temperatures. Assuming 4500 kg/day, a 7 m^2 rotary cooler will be required according to the calculations of McCabe et al. [93] to achieve a temperature drop from 700 °C to room temperature in less than 1 h. The cooled activated carbon should be washed with distilled water to remove residual potassium hydroxide. The washing process will take place in a reactor with a capacity of 8000 L, using 40 L of water per kilogram of carbon. Then, feed the material into an 8000 L reactor with 1 M hydrochloric acid, using 10 L of acid per kilogram of carbon. The water washing process is repeated to remove residual HCl in an 8000 L reactor using 40 L of water per kilogram of carbon. The final step is collecting the carbon on a dewatering sieve and transferring it to a rotary dryer. Assuming a process load of 5000 kg of wet carbon and using the data provided by McCabe et al. [93], a 1.24–2.15 m rotary dryer will be needed. Similarly as before, in order to avoid rusting, it is recommended to be made of stainless steel. Finally, the weight loss from screening is estimated to be up to 5%. Hence, the final weight of the resulting product is 3325 kg/day.

The production cost was calculated assuming 30% efficiency or 3325 kg/day of activated carbon production. The production time is 320 days/year in a three-shift system for 24 h with 3 employees and € 4.20 per hour. An investment of € 4.6 million is required for the activation of potassium hydroxide (Table 8). The annual production cost is estimated to be € 2.24 million (Table 9) with an annual production of 1.064.000 kg. The estimated cost per kilogram of activated carbon would be € 2.10 (Table 10). The project does not include energy recovery devices.

The estimated cost of producing activated carbon from surgical masks is 2.10 €/kg and may compete with other activated carbons obtained from waste materials. Ng et al. [95] obtained activated carbon based on pecan shells and estimated the cost of its production at € 2.34–2.49 per kilogram depending on the type of material activation. On the other hand, Lima et al. [96] prepared activated carbon from the body waste through physical activation and calculated that the cost of production at zero raw material price was € 1.24. Stavropoulos et al. [97] reported the production costs of activated carbon obtained from used tires, wood, and lignite to be 9.81 €/kg, 5.49 €/kg and 4.62 €/kg,

Table 8
Estimated capital costs.

Equipment	Cost (€)
Cutting machine	6880
Storage tank	68,800
Rotary dryer	130,000
Tube furnace	176,000
Rotary cooler	85,000
2 tanks for water washing	140,000
1 tank to acid washing	70,000
Rotary dryer	130,000
Sieve	2600
Total equipment cost	809,280
Equipment installation	453,000
Instrumentation	349,000
Material transport	397,000
Electrical installation	250,000
Buildings	250,000
Yard improvements	98,000
Service	750,500
Land	49,000
Engineering and supervision	501,400
Construction expense	599,000
Contractor's fee	98,000
Contingency	395,000
Total capital costs	4,602,180

*Capital costs based on different percentages of the total equipment cost according to Peters and Timmerhaus [94].

Table 9
Annual operating costs.

Item Raw material	Annual cost (€)
Chirurgical masks	30,000
Potassium hydroxide	220,000
Nitrogen	10,000
Utilities	
Water	30,000
Electricity	65,000
Natural gas	30,000
Labor	
Operating labor	325,000
Maintenance labor	100,000
Supervision	60,000
Fringe benefits	162,000
Supplies	
Operating supplies	40,000
Maintenance supplies	54,000
General works	
General and administrative	40,000
Property insurance and tax	35,000
Depreciation	40,000
Total cost	2,241,000

*Annual operating costs for labor, supplies and general work are based on percentages given in Peters and Timmerhaus [94].

Table 10
Summary of costs.

Purchased equipment cost[a]	809,280 €
Capital cost[a]	3,792,900 €
Total fixed capital investment[b]	4,602,180 €
Total annual operating cost[c]	2,241,000 €
Estimated annual production of carbon[d]	1,528,000 kg
Estimated cost for activated carbon	€ **2.10 per kg**

[a] Table 7.
[b] Total capital costs.
[c] Table 8.
[d] Based on a 4775 kg/day output and 320 day/year production.

respectively.

5. Conclusions

The high-value-added activated carbons produced from disposable face masks have been investigated and described for the first time. The disposable face masks are waste associated with their increased use, especially during a viral epidemic. The obtained carbon was characterized in N_2 and CO_2 sorption investigations and with SEM, XRD, and Raman spectroscopy. XRD results revealed the amorphous nature of the samples, which was confirmed by Raman spectroscopy.

The carbons produced from masks possessed a high surface area and narrow pore distribution which made them a highly efficient candidate for CO_2 adsorbent. The highest CO_2 adsorption was observed on carbon produced at 800 °C. The adsorption of carbon dioxide of this sample at 1 bar was 3.91 mmol/g, 3.23 mmol/g and 2.61 mmol/g at 0 °C, 10 °C and 20 °C, respectively. CO_2 adsorption was most dependent on micropores in the range of 0.4–1 nm. The selectivity of separation for CO_2 over N_2 was calculated based on IAST for equimolar CO_2 and N_2 binary mixture, for flue gas composition and also using the ratios of the Henry's law constants. The selectivity values on M_800 were the highest so far described in the literature. The overall results suggest that activated carbons produced from disposable face masks can be applied as potential adsorbents for CO_2 separation. Therefore, the approach presented here, which relies on carbonization combined with chemical activation, is an easy method using cheap carbon sources that could be a promising and practical alternative for CO_2 adsorption. That is why it is so important that used face masks could be easily and safely transformed into a full-value product, an effective adsorbent in many processes. Finally, our idea of managing waste masks can be an easy way of decreasing the amount of generated plastic waste.

CRediT authorship contribution statement

Jarosław Serafin: Conceptualization, Methodology, Validation, Formal analysis, Investigation, Data curation, Writing – original draft, Writing – review and editing, Visualization, supervision. **Joanna Sreńscek-Nazzal:** Conceptualization, Methodology, Formal analysis, Investigation, Data curation, Writing – original draft, Writing – review and editing, Visualization. **Adrianna Kamińska:** Methodology, Formal analysis, Investigation, Data curation, Writing – original draft, Writing – review and editing, Visualization. **Oliwia Paszkiewicz:** Investigation, Writing – original draft, Writing – review and editing. **Beata Michalkiewicz:** Validation, Data curation, Writing – original draft, Writing – review and editing, Supervision. All authors have read and agreed to the published version of the manuscript.

Declaration of Competing Interest

The authors declare that they have no known competing financial interests or personal relationships that could have appeared to influence the work reported in this paper.

Acknowledgments

The authors are grateful for the scientific discussion and help of Professor Agata Markowska-Szczupak.

Conflicts of interest

The authors declare no conflict of interest.

References

[1] G.N. Muriithi, L.F. Petrik, F.J. Doucet, Synthesis, characterisation and CO_2 adsorption potential of NaA and NaX zeolites and hydrotalcite obtained from the

same coal fly ash, J. CO2 Util. 36 (2020) 220–230, https://doi.org/10.1016/j.jcou.2019.11.016.
[2] J. Kapica-Kozar, E. Piróg, E. Kusiak-Nejman, R.J. Wrobel, A. Gęsikiewicz-Puchalska, A.W. Morawski, U. Narkiewicz, B. Michalkiewicz, Titanium dioxide modified with various amines used as sorbents of carbon dioxide, New J. Chem. 41 (2017) 1549–1557, https://doi.org/10.1039/C6NJ02808J.
[3] A.H. Assen, Y. Belmabkhout, K. Adil, A. Lachehab, H. Hassoune, H. Aggarwal, Advances on CO_2 storage. Synthetic porous solids, mineralization and alternative solutions, Chem. Eng. J. 419 (2021), 129569, https://doi.org/10.1016/j.cej.2021.129569.
[4] B. Zielinska, B. Michalkiewicz, X. Chen, E. Mijowska, R.J. Kalenczuk, Pd supported ordered mesoporous hollow carbon spheres (OMHCS) for hydrogen storage, Chem. Phys. Lett. 647 (2016) 14–19, https://doi.org/10.1016/j.cplett.2016.01.036.
[5] N. Balahmar, A.S. Al-Jumialy, R. Mokaya, Biomass to porous carbon in one step: Directly activated biomass for high performance CO_2 storage, J. Mater. Chem. A 5 (2017) 12330–12339, https://doi.org/10.1039/c7ta01722g.
[6] A. Sayari, Y. Belmabkhout, R. Serna-Guerrero, Flue gas treatment via CO_2 adsorption, Chem. Eng. J. 171 (2011) 760–774, https://doi.org/10.1016/j.cej.2011.02.007.
[7] J. Jänchen, D.T.F. Möhlmann, H. Stach, Water and carbon dioxide sorption properties of natural zeolites and clay minerals at martian surface temperature and pressure conditions, Stud. Surf. Sci. Catal. (2007) 2116–2121, https://doi.org/10.1016/S0167-2991(07)81108-6.
[8] A. Ertan, F. Çakicioğlu-Özkan, CO2 and N2 adsorption on the acid (HCl, HNO3, H2SO4 and H3PO4) treated zeolites, Adsorption 11 (2005) 151–156, https://doi.org/10.1007/s10450-005-5914-7.
[9] D.M. D'Alessandro, B. Smit, J.R. Long, Carbon dioxide capture: prospects for new materials, Angew. Chem. Int. Ed. 49 (2010) 6058–6082, https://doi.org/10.1002/anie.201000431.
[10] A. Samanta, A. Zhao, G.K.H. Shimizu, P. Sarkar, R. Gupta, Post-combustion CO 2 capture using solid sorbents: a review, Ind. Eng. Chem. Res. 51 (2012) 1438–1463, https://doi.org/10.1021/ie200686q.
[11] Q. Wang, J. Luo, Z. Zhong, A. Borgna, CO_2 capture by solid adsorbents and their applications: current status and new trends, Energy Environ. Sci. 4 (2011) 42–55, https://doi.org/10.1039/c0ee00064g.
[12] F.V.S. Lopes, C.A. Grande, A.M. Ribeiro, J.M. Loureiro, O. Evaggelos, V. Nikolakis, A.E. Rodrigues, Adsorption of H2, CO_2, CH4, CO, N2 and H2O in activated carbon and zeolite for hydrogen production, Sep. Sci. Technol. 44 (2009) 1045–1073, https://doi.org/10.1080/01496390902729130.
[13] M.M. Dubinin, Adsorption properties and microporous structures of carbonaceous adsorbents, Carbon 25 (1987) 593–598, https://doi.org/10.1016/0008-6223(87)90208-9.
[14] C. Voss, Applications of pressure swing adsorption technology, Adsorption 11 (2005) 527–529, https://doi.org/10.1007/s10450-005-5979-3.
[15] V.G. Gomes, K.W.K. Yee, Pressure swing adsorption for carbon dioxide sequestration from exhaust gases, Sep. Purif. Technol. 28 (2002) 161–171, https://doi.org/10.1016/S1383-5866(02)00064-3.
[16] N. Tlili, G. Grévillot, C. Vallières, Carbon dioxide capture and recovery by means of TSA and/or VSA, Int. J. Greenh. Gas Control. 3 (2009) 519–527, https://doi.org/10.1016/j.ijggc.2009.04.005.
[17] P. Ammendola, F. Raganati, R. Chirone, F. Miccio, Fixed bed adsorption as affected by thermodynamics and kinetics: Yellow tuff for CO_2 capture, Powder Technol. 373 (2020) 446–458, https://doi.org/10.1016/j.powtec.2020.06.075.
[18] F. Raganati, F. Miccio, P. Ammendola, Adsorption of carbon dioxide for post-combustion capture: a review, Energy Fuels 35 (2021) 12845–12868, https://doi.org/10.1021/acs.energyfuels.1c01618.
[19] C. Dhoke, A. Zaabout, S. Cloete, S. Amini, Review on reactor configurations for adsorption-based CO_2 capture, Ind. Eng. Chem. Res. 60 (2021) 3779–3798, https://doi.org/10.1021/acs.iecr.0c04547.
[20] J. Shabanian, R. Jafari, J. Chaouki, Fluidization of ultrafine powders, Int. Rev. Chem. Eng. 4 (2012) 16–50.
[21] F. Raganati, P. Ammendola, Sound-assisted fluidization for temperature swing adsorption and calcium looping: a review, Materials (2021) 1–24, https://doi.org/10.3390/ma14030672.
[22] V. Gargiulo, M. Alfè, P. Ammendola, F. Raganati, R. Chirone, CO2 sorption on surface-modified carbonaceous support: probing the influence of the carbon black microporosity and surface polarity, Appl. Surf. Sci. 360 (2016) 329–337, https://doi.org/10.1016/j.apsusc.2015.11.026.
[23] M. Alfe, P. Ammendola, V. Gargiulo, F. Raganati, R. Chirone, Magnetite loaded carbon fine particles as low-cost CO_2 adsorbent in a sound assisted fluidized bed, Proc. Combust. Inst. 35 (2015) 2801–2809, https://doi.org/10.1016/j.proci.2014.06.037.
[24] D. Saha, M.J. Kienbaum, Role of oxygen, nitrogen and sulfur functionalities on the surface of nanoporous carbons in CO_2 adsorption: a critical review, Microporous Mesoporous Mater. 287 (2019) 29–55, https://doi.org/10.1016/j.micromeso.2019.05.051.
[25] M.A. Izquierdo-Barrientos, C. Sobrino, J.A. Almendros-Ibáñez, Experimental heat transfer coefficients between a surface and fixed and fluidized beds with PCM, Appl. Therm. Eng. 78 (2015) 373–379, https://doi.org/10.1016/j.applthermaleng.2014.12.044.
[26] F. Raganati, R. Chirone, P. Ammendola, Gas-solid fluidization of cohesive powders, Chem. Eng. Res. Des. 133 (2018) 347–387, https://doi.org/10.1016/j.cherd.2018.03.034.
[27] F. Raganati, R. Chirone, P. Ammendola, Effect of temperature on fluidization of Geldart's group A and C powders: role of interparticle forces, Ind. Eng. Chem. Res. 56 (2017) 12811–12821, https://doi.org/10.1021/acs.iecr.7b03270.
[28] P. Ammendola, R. Chirone, F. Raganati, Fluidization of binary mixtures of nanoparticles under the effect of acoustic fields, Adv. Powder Technol. 22 (2011) 174–183, https://doi.org/10.1016/j.apt.2010.10.002.
[29] M. Grundy, Z. Ye, Cross-linked polymers of diethynylbenzene and phenylacetylene as new polymer precursors for high-yield synthesis of high-performance nanoporous activated carbons for supercapacitors, hydrogen storage, and CO_2 capture, J. Mater. Chem. A 2 (2014) 20316–20330, https://doi.org/10.1039/c4ta04038d.
[30] Y. Yang, P. Shukla, S. Wang, V. Rudolph, X.-M. Chen, Z. Zhu, Significant improvement of surface area and CO_2 adsorption of Cu–BTC via solvent exchange activation, RSC Adv. 3 (2013) 17065, https://doi.org/10.1039/c3ra42519c.
[31] J. Serafin, M. Baca, M. Biegun, E. Mijowska, R.J. Kaleńczuk, J. Sreńscek-Nazzal, B. Michalkiewicz, Direct conversion of biomass to nanoporous activated biocarbons for high CO_2 adsorption and supercapacitor applications, Appl. Surf. Sci. 497 (2019), 143722, https://doi.org/10.1016/j.apsusc.2019.143722.
[32] H. Wei, S. Deng, B. Hu, Z. Chen, B. Wang, J. Huang, G. Yu, Granular bamboo-derived activated carbon for high CO2 adsorption: the dominant role of narrow micropores, ChemSusChem 5 (2012) 2354–2360, https://doi.org/10.1002/cssc.201200570.
[33] J. Serafin, M. Ouzzine, O.F. Cruz Junior, J. Sreńscek-Nazzal, Preparation of low-cost activated carbons from amazonian nutshells for CO_2 storage, Biomass Bioenergy 144 (2021), 105925, https://doi.org/10.1016/j.biombioe.2020.105925.
[34] M. Ouzzine, J. Serafin, J. Sreńscek-Nazzal, Single step preparation of activated biocarbons derived from pomegranate peels and their CO_2 adsorption performance, J. Anal. Appl. Pyrolysis 160 (2021), 105338, https://doi.org/10.1016/j.jaap.2021.105338.
[35] S. Rattanaphan, T. Rungrotmongkol, P. Kongsune, Biogas improving by adsorption of CO_2 on modified waste tea activated carbon, Renew. Energy 145 (2020) 622–631, https://doi.org/10.1016/j.renene.2019.05.104.
[36] J. Patiño, M.C. Gutiérrez, D. Carriazo, C.O. Ania, J.B. Parra, M.L. Ferrer, F. del Monte, Deep eutectic assisted synthesis of carbon adsorbents highly suitable for low-pressure separation of CO_2–CH4 gas mixtures, Energy Environ. Sci. 5 (2012) 8699, https://doi.org/10.1039/c2ee22029f.
[37] M. Sevilla, A.B. Fuertes, Sustainable porous carbons with a superior performance for CO_2 capture, Energy Environ. Sci. 4 (2011) 1765–1771, https://doi.org/10.1039/c0ee00784f.
[38] S. Saadat, D. Rawtani, C.M. Hussain, Environmental perspective of COVID-19, Sci. Total Environ. 728 (2020), 138870, https://doi.org/10.1016/j.scitotenv.2020.138870.
[39] J. Peng, X. Wu, R. Wang, C. Li, Q. Zhang, D. Wei, Medical waste management practice during the 2019-2020 novel coronavirus pandemic: experience in a general hospital, Am. J. Infect. Control 48 (2020) 918–921, https://doi.org/10.1016/j.ajic.2020.05.035.
[40] S. Dharmaraj, V. Ashokkumar, S. Hariharan, A. Manibharathi, P.L. Show, C. T. Chong, C. Ngamcharussrivichai, The COVID-19 pandemic face mask waste: a blooming threat to the marine environment, Chemosphere 272 (2021), 129601, https://doi.org/10.1016/j.chemosphere.2021.129601.
[41] S.B. Lee, J. Lee, Y.F. Tsang, Y.M. Kim, J. Jae, S.C. Jung, Y.K. Park, Production of value-added aromatics from wasted COVID-19 mask via catalytic pyrolysis, Environ. Pollut. 283 (2021), 117060, https://doi.org/10.1016/j.envpol.2021.117060.
[42] C. Park, H. Choi, K.Y. Andrew Lin, E.E. Kwon, J. Lee, COVID-19 mask waste to energy via thermochemical pathway: effect of co-feeding food waste, Energy 230 (2021), 120876, https://doi.org/10.1016/j.energy.2021.120876.
[43] J. Sreńscek-Nazzal, U. Narkiewicz, A.W. Morawski, R.J. Wróbel, B. Michalkiewicz, Comparison of optimized isotherm models and error functions for carbon dioxide adsorption on activated carbon, J. Chem. Eng. Data 60 (2015) 3148–3158, https://doi.org/10.1021/acs.jced.5b00294.
[44] W. Tongpoothorn, M. Sriuttha, P. Homchan, S. Chanthai, C. Ruangviriyachai, Preparation of activated carbon derived from Jatropha curcas fruit shell by simple thermo-chemical activation and characterization of their physico-chemical properties, Chem. Eng. Res. Des. 89 (2011) 335–340, https://doi.org/10.1016/j.cherd.2010.06.012.
[45] C. Pechyen, D. Atong, D. Aht-Ong, V. Sricharoenchaikul, Investigation of pyrolyzed chars from physic nut waste for the preparation of activated carbon, J. Solid Mech. Mater. Eng. 1 (2007) 498–507, https://doi.org/10.1299/jmmp.1.498.
[46] L. Wang, C. Tian, B. Wang, R. Wang, W. Zhou, H. Fu, Controllable synthesis of graphitic carbon nanostructures from ion-exchange resin-iron complex via solid-state pyrolysis process, Chem. Commun. (2008) 5411, https://doi.org/10.1039/b810500f.
[47] D. Liu, B. Xu, J. Zhu, S. Tang, F. Xu, S. Li, B. Jia, G. Chen, Preparation of highly porous graphitic activated carbon as electrode materials for supercapacitors by hydrothermal pretreatment-assisted chemical activation, ACS Omega 5 (2020) 11058–11067, https://doi.org/10.1021/acsomega.0c00938.
[48] J. Sreńscek-Nazzal, K. Kiełbasa, Advances in modification of commercial activated carbon for enhancement of CO_2 capture, Appl. Surf. Sci. 494 (2019) 137–151, https://doi.org/10.1016/j.apsusc.2019.07.108.
[49] C.F. Martín, M.G. Plaza, S. García, J.J. Pis, F. Rubiera, C. Pevida, Microporous phenol-formaldehyde resin-based adsorbents for pre-combustion CO_2 capture, Fuel 90 (2011) 2064–2072, https://doi.org/10.1016/j.fuel.2011.01.019.
[50] N.P. Wickramaratne, M. Jaroniec, Importance of small micropores in CO_2 capture by phenolic resin-based activated carbon spheres, J. Mater. Chem. A 1 (2013) 112–116, https://doi.org/10.1039/c2ta00388k.
[51] K. Li, S. Tian, J. Jiang, J. Wang, X. Chen, F. Yan, Pine cone shell-based activated carbon used for CO_2 adsorption, J. Mater. Chem. A 4 (2016) 5223–5234, https://doi.org/10.1039/c5ta09908k.

[52] R.F. Weiner, R.A. Matthews. Environmental Engineering, fourth ed., Elsevier, 2003 https://doi.org/10.1016/B978-0-7506-7294-8.X5000-3.

[53] S. Timur, I.C. Kantarli, S. Onenc, J. Yanik, Characterization and application of activated carbon produced from oak cups pulp, J. Anal. Appl. Pyrolysis 89 (2010) 129–136, https://doi.org/10.1016/j.jaap.2010.07.002.

[54] A. Heidari, H. Younesi, A. Rashidi, A. Ghoreyshi, Adsorptive removal of CO_2 on highly microporous activated carbons prepared from Eucalyptus camaldulensis wood: effect of chemical activation, J. Taiwan Inst. Chem. Eng. 45 (2014) 579–588, https://doi.org/10.1016/j.jtice.2013.06.007.

[55] J. Chen, L. Zhang, G. Yang, Q. Wang, R. Li, L.A. Lucia, Preparation and characterization of activated carbon from hydrochar by phosphoric acid activation and its adsorption performance in prehydrolysis liquor, BioResources 12 (2017), https://doi.org/10.15376/biores.12.3.5928-5941.

[56] J. Serafin, K. Kiełbasa, B. Michalkiewicz, The new tailored nanoporous carbons from the common polypody (Polypodium vulgare): the role of textural properties for enhanced CO_2 adsorption, Chem. Eng. J. 429 (2022), 131751, https://doi.org/10.1016/j.cej.2021.131751.

[57] S.M.W. Wilson, F. Al-Enzi, V.A. Gabriel, F.H. Tezel, Effect of pore size and heterogeneous surface on the adsorption of CO_2, N2, O2, and Ar on carbon aerogel, RF aerogel, and activated carbons, Microporous Mesoporous Mater. 322 (2021), 111089, https://doi.org/10.1016/j.micromeso.2021.111089.

[58] M. Alhassan, M. Auta, J. Sabo, M. Umaru, A. Kovo, CO_2 capture using amine-impregnated activated carbon from jatropha curcas shell, Br. J. Appl. Sci. Technol. 14 (2016) 1–11, https://doi.org/10.9734/bjast/2016/24253.

[59] R. Sabouni, H. Kazemian, S. Rohani, Carbon dioxide adsorption in microwave-synthesized metal organic framework CPM-5: equilibrium and kinetics study, Microporous Mesoporous Mater. 175 (2013) 85–91, https://doi.org/10.1016/j.micromeso.2013.03.024.

[60] M. Thommes, K. Kaneko, A.V. Neimark, J.P. Olivier, F. Rodriguez-Reinoso, J. Rouquerol, K.S.W. Sing, Physisorption of gases, with special reference to the evaluation of surface area and pore size distribution (IUPAC technical report), Pure Appl. Chem. 87 (2015) 1051–1069, https://doi.org/10.1515/pac-2014-1117.

[61] S. Makhseed, J. Samuel, Imide-linked microporous organic framework polymers for CO_2 adsorption, Polymer 74 (2015) 144–149, https://doi.org/10.1016/j.polymer.2015.07.057.

[62] F.J. Martín-Jimeno, F. Suárez-García, J.I. Paredes, A. Martínez-Alonso, J.M. D. Tascón, Activated carbon xerogels with a cellular morphology derived from hydrothermally carbonized glucose-graphene oxide hybrids and their performance towards CO_2 and dye adsorption, Carbon 81 (2015) 137–147, https://doi.org/10.1016/j.carbon.2014.09.042.

[63] J. Lu, C. Jiao, Z. Majeed, H. Jiang, Magnesium and nitrogen co-doped mesoporous carbon with enhanced microporosity for CO_2 adsorption, Nanomaterials 8 (2018) 275, https://doi.org/10.3390/nano8050275.

[64] Y. Li, R. Xu, X. Wang, B. Wang, J. Cao, J. Yang, J. Wei, Waste wool derived nitrogen-doped hierarchical porous carbon for selective CO2 capture, RSC Adv. 8 (2018) 19818–19826, https://doi.org/10.1039/C8RA02701C.

[65] J. Serafin, M. Ouzzine, O.F. Cruz, J. Sreńscek-Nazzal, I. Campello Gómez, F.-Z. Azar, C.A. Rey Mafull, D. Hotza, C.R. Rambo, Conversion of fruit waste-derived biomass to highly microporous activated carbon for enhanced CO_2 capture, Waste Manag. 136 (2021) 273–282, https://doi.org/10.1016/j.wasman.2021.10.025.

[66] D.P. Vargas, L. Giraldo, A. Erto, J.C. Moreno-Piraján, Chemical modification of activated carbon monoliths for CO_2 adsorption, J. Therm. Anal. Calorim. 114 (2013) 1039–1047, https://doi.org/10.1007/s10973-013-3086-3.

[67] J. Choma, M. Marszewski, L. Osuchowski, J. Jagiello, A. Dziura, M. Jaroniec, Adsorption properties of activated carbons prepared from waste CDs and DVDs, ACS Sustain. Chem. Eng. 3 (2015) 733–742, https://doi.org/10.1021/acssuschemeng.5b00036.

[68] B. Yuan, X. Wu, Y. Chen, J. Huang, H. Luo, S. Deng, Adsorption of CO2, CH4, and N2 on ordered mesoporous carbon: approach for greenhouse gases capture and biogas upgrading, Environ. Sci. Technol. 47 (2013) 5474–5480, https://doi.org/10.1021/es4000643.

[69] Z.Y. Sui, Q.H. Meng, J.T. Li, J.H. Zhu, Y. Cui, B.H. Han, High surface area porous carbons produced by steam activation of graphene aerogels, J. Mater. Chem. A 2 (2014) 9891–9898, https://doi.org/10.1039/c4ta01387e.

[70] G.K. Parshetti, S. Chowdhury, R. Balasubramanian, Biomass derived low-cost microporous adsorbents for efficient CO_2 capture, Fuel 148 (2015) 246–254, https://doi.org/10.1016/j.fuel.2015.01.032.

[71] K.K. Kishibayev, J. Serafin, R.R. Tokpayev, T.N. Khavaza, A.A. Atchabarova, D. A. Abduakhytova, Z.T. Ibraimov, J. Sreńscek-Nazzal, Physical and chemical properties of activated carbon synthesized from plant wastes and shungite for CO_2 capture, J. Environ. Chem. Eng. 9 (2021), 106798, https://doi.org/10.1016/j.jece.2021.106798.

[72] T. Chen, S. Deng, B. Wang, J. Huang, Y. Wang, G. Yu, CO_2 adsorption on crab shell derived activated carbons: contribution of micropores and nitrogen-containing groups, RSC Adv. 5 (2015) 48323–48330, https://doi.org/10.1039/c5ra04937g.

[73] S. Deng, H. Wei, T. Chen, B. Wang, J. Huang, G. Yu, Superior CO_2 adsorption on pine nut shell-derived activated carbons and the effective micropores at different temperatures, Chem. Eng. J. 253 (2014) 46–54, https://doi.org/10.1016/j.cej.2014.04.115.

[74] V. Presser, J. McDonough, S.H. Yeon, Y. Gogotsi, Effect of pore size on carbon dioxide sorption by carbide derived carbon, Energy Environ. Sci. 4 (2011) 3059–3066, https://doi.org/10.1039/c1ee01176f.

[75] J.M. Martín-Martínez, R. Torregrosa-Maciá, M.C. Mittelmeijer-Hazeleger, Mechanisms of adsorption of CO_2 in the micropores of activated anthracite, Fuel 74 (1995) 111–114, https://doi.org/10.1016/0016-2361(94)P4340-8.

[76] A. Vishnyakov, P.I. Ravikovitch, A.V. Neimark, Molecular level models for CO_2 sorption in nanopores, Langmuir 15 (1999) 8736–8742, https://doi.org/10.1021/la990726c.

[77] Y. Guo, C. Tan, J. Sun, W. Li, J. Zhang, C. Zhao, Porous activated carbons derived from waste sugarcane bagasse for CO_2 adsorption, Chem. Eng. J. 381 (2020), 122736, https://doi.org/10.1016/j.cej.2019.122736.

[78] K. Kiełbasa, J. Sreńscek-Nazzal, B. Michalkiewicz, Impact of tailored textural properties of activated carbons on methane storage, Powder Technol. 394 (2021) 336–352, https://doi.org/10.1016/j.powtec.2021.08.051.

[79] A.L. Myers, J.M. Prausnitz, Thermodynamics of mixed-gas adsorption, AIChE J. 11 (1965) 121–127, https://doi.org/10.1002/aic.690110125.

[80] F. Xu, Y. Yu, J. Yan, Q. Xia, H. Wang, J. Li, Z. Li, Ultrafast room temperature synthesis of GrO@HKUST-1 composites with high CO_2 adsorption capacity and CO_2/N2 adsorption selectivity, Chem. Eng. J. 303 (2016) 231–237, https://doi.org/10.1016/j.cej.2016.05.143.

[81] J.A. Mason, K. Sumida, Z.R. Herm, R. Krishna, J.R. Long, Evaluating metal-organic frameworks for post-combustion carbon dioxide capture via temperature swing adsorption, Energy Environ. Sci. 4 (2011) 3030–3040, https://doi.org/10.1039/c1ee01720a.

[82] S. Li, Y.G. Chung, R.Q. Snurr, High-throughput screening of metal–organic frameworks for CO2 capture in the presence of water, Langmuir 32 (2016) 10368–10376, https://doi.org/10.1021/acs.langmuir.6b02803.

[83] M. Saleh, J.N. Tiwari, K.C. Kemp, M. Yousuf, K.S. Kim, Highly selective and stable carbon dioxide uptake in polyindole-derived microporous carbon materials, Environ. Sci. Technol. 47 (2013) 5467–5473, https://doi.org/10.1021/es3052922.

[84] M. Saleh, V. Chandra, K. Christian Kemp, K.S. Kim, Synthesis of N-doped microporous carbon via chemical activation of polyindole-modified graphene oxide sheets for selective carbon dioxide adsorption, Nanotechnology 24 (2013), 255702, https://doi.org/10.1088/0957-4484/24/25/255702.

[85] A.S. González, M.G. Plaza, F. Rubiera, C. Pevida, Sustainable biomass-based carbon adsorbents for post-combustion CO_2 capture, Chem. Eng. J. 230 (2013) 456–465, https://doi.org/10.1016/j.cej.2013.06.118.

[86] J. Wang, A. Heerwig, M.R. Lohe, M. Oschatz, L. Borchardt, S. Kaskel, Fungi-based porous carbons for CO 2 adsorption and separation, J. Mater. Chem. 22 (2012) 13911–13913, https://doi.org/10.1039/c2jm32139d.

[87] A. Wahby, J.M. Ramos-Fernández, M. Martínez-Escandell, A. Sepúveda-Escribano, J. Silvestre-Albero, F. Rodríguez-Reinoso, High-surface-area carbon molecular sieves for selective CO_2 adsorption, ChemSusChem 3 (2010) 974–981, https://doi.org/10.1002/cssc.201000083.

[88] J. Wang, Q. Liu, An efficient one-step condensation and activation strategy to synthesize porous carbons with optimal micropore sizes for highly selective CO_2 adsorption, Nanoscale 6 (2014) 4148–4156, https://doi.org/10.1039/c3nr05825e.

[89] L.H. Xie, M.P. Suh, High CO_2-capture ability of a porous organic polymer bifunctionalized with carboxy and triazole groups, Chem. Eur. J. 19 (2013) 11590–11597, https://doi.org/10.1002/chem.201301822.

[90] X. Fan, L. Zhang, G. Zhang, Z. Shu, J. Shi, Chitosan derived nitrogen-doped microporous carbons for high performance CO_2 capture, Carbon 61 (2013) 423–430, https://doi.org/10.1016/j.carbon.2013.05.026.

[91] M. Sevilla, C. Falco, M.M. Titirici, A.B. Fuertes, High-performance CO_2 sorbents from algae, RSC Adv. 2 (2012) 12792–12797, https://doi.org/10.1039/c2ra22552b.

[92] E.K. Jeong, J.E. Bae, I.S. Kim, Inactivation of influenza A virus H1N1 by disinfection process, Am. J. Infect. Control 38 (2010) 354–360, https://doi.org/10.1016/j.ajic.2010.03.003.

[93] W. McCabe, J. Smith, P. Harriott, Unit Operations of Chemical Engineering, McGraw-Hill Education, New York, 2005. ⟨https://books.google.pl/books?id=u3SvHtIOwj8C⟩.

[94] M.S. Peters, J.I. Peters, Plant Design and Economics for Chemical Engineers, McGraw-Hill Education, 1959, https://doi.org/10.1080/00137915908965075.

[95] C. Ng, W.E. Marshall, R.M. Rao, R.R. Bansode, J.N. Losso, Activated carbon from pecan shell: process description and economic analysis, Ind. Crop. Prod. 17 (2003) 209–217, https://doi.org/10.1016/S0926-6690(03)00002-5.

[96] I.M. Lima, A. McAloon, A.A. Boateng, Activated carbon from broiler litter: process description and cost of production, Biomass Bioenergy 32 (2008) 568–572, https://doi.org/10.1016/j.biombioe.2007.11.008.

[97] G.G. Stavropoulos, A.A. Zabaniotou, Minimizing activated carbons production cost, Fuel Process. Technol. 90 (2009) 952–957, https://doi.org/10.1016/j.fuproc.2009.04.002.